PERFORMANCE ANALYSIS OF DIFFERENT SCHEMES FOR TRANSMISSION OF WATERMARKED MEDICAL IMAGES OVER FADING CHANNELS

Praveen Kumar Korrai

A THESIS

IN

THE DEPARTMENT

OF

ELECTRICAL AND COMPUTER ENGINEERING

PRESENTED IN PARTIAL FULFILLMENT OF THE REQUIREMENTS
FOR THE DEGREE OF MASTER OF APPLIED SCIENCES
CONCORDIA UNIVERSITY
MONTREAL, QUEBEC, CANADA
AUGUST 2013

CONCORDIA UNIVERSITY

School of Graduate Studies

This is to certify that the thesis prepared

By: Praveen Kumar Korrai

Entitled: Performance Analysis of Different Schemes for Transmission of Watermarked Medical images over Fading Channels.

and submitted in partial fulfillment of the requirements for the degree of

Master of applied sciences (Electrical and Computer Engineering)

complies with the regulations of the University and meets the accepted standards with respect to originality and quality.

Signed by the final examining Committee:

_____ Chair
Dr. Robin Raut

_____ Examiner
Dr. Chun-Yi Su

_____ Examiner
Dr. M. O. Ahmad

_____ Supervisor
Dr. M. N. S. Swamy

Approved by   _____
                Dr. Abdel R Sebak,   Graduate Program Director 2013

                _____

                Dr. Christopher Trueman, Interim Dean
                Faculty of Engineering and Computer Science

ABSTRACT

Performance Analysis of Different Schemes for Transmission of Watermarked Medical images over Fading Channels

Praveen Kumar Korrai

In this thesis, we investigate different types of robust schemes for transmission of medical images with concealed patient information as a watermark. In these schemes, spatial domain digital watermarking technique is adapted to embed the patient information as a watermark into the lower order bits of the medical images to reduce the storage and transmission overheads. The watermark, which comprises text data, is encrypted to prevent unauthorized access of data. To enhance the robustness of the embedded information, the encrypted watermark is coded by concatenation of Reed Solomon (RS) and low density parity check (LDPC) codes. A robust scheme for transmission of watermarked images over impulsive noisy wireless channels is first proposed and its performance analyzed. In this scheme, the bursty wireless channel is simulated by adding impulse noise to the watermark embedded image. Furthermore, turbo channel coding is used to correct the transmission errors over impulsive noisy wireless channels.

However, single input single output (SISO) channel capacity is not enough to provide modern wireless services such as data and multimedia messaging services. Further, it is not reliable due to multipath fading. To overcome these problems, a multiple-input multiple-output (MIMO) transmission scheme in which multiple antennas are used at both the transmitter and the receiver has emerged as one of the most significant technical breakthroughs in modern wireless

communications. MIMO can improve the channel capacity and provide diversity gain. Hence, a scheme with a MIMO channel is proposed for the transmission of watermarked medical images over Rayleigh flat fading channels and its performance analyzed using MIMO maximum likelihood detector at the receiver.

We present another scheme, namely, MIMO space frequency block coded OFDM (MIMO SFBC OFDM) in this thesis for transmission of watermarked medical images over Rayleigh fading channels to mitigate the detrimental effects due to frequency selective fading. The performance of this MIMO SFBC OFDM scheme is analyzed and compared with that of SISO-OFDM using minimum mean square error V-BLAST- based detection at the receiver.

The efficacy of the different proposed schemes is illustrated through implementation results on watermarked medical images.

Aapadam Apa Hartharam Dhataram Sarva Sampadam,
Lokabhi Ramam Sri Ramam Bhooyo Bhooyo Namamyaham.

Sri Rama Rama Rameti, Rame Raame Manorame
Sahasra Nama Tat Tulyam, Rama Nama Varanane!

ACKNOWLEDGEMENT

First and foremost, I would like to express my deepest gratitude to my supervisor, Dr. M. N. S. Swamy, for his valuable guidance and support throughout the span of this research. He has been extremely encouraging and extraordinarily patient throughout my graduate study. I sincerely thank him for his interpretation of the texts in numerous places and teaching me the nuances of expressions while editing the report without which I could not have completed this submission.

I would like to thank Dr. Omair Ahmad, Dr. Weiping Zhu, and Dr. Yousef Shayan for insightful discussions on related topics at one point or other during my course work. Studies of this nature would have been impossible without access to related books, journals and other works of reference. I take this time to thank Concordia library for assisting me with the necessary sources of references.

I would like to thank my friends: Aravind Voruganti, Sukesh Reddy, Chiranjeevi, Sarath Somasekharan Pillai, Sony prattipati, Arun Reddy and Abdallah Elayan for making my graduate experience memorable and being like a family.

Finally, and most importantly, I would like to thank my parents Rama Rao and Lokeswari, my other family members, and relatives for their love, support and encouragement during my studies. Special thanks to my uncle, Dr. K. Deergha Rao, whose love, unlimited support, and encouragement have made the successful completion of this thesis a reality.

Dedicated to my loving family…………………………..

TABLE OF CONTENTS

LIST OF FIGURES

LIST OF TABLES

LIST OF SYMBOLS

B_c : Coherence bandwidth

B_D : Doppler spread of the channel.

B_s : Bandwidth of the transmitted signal

C_{AWGN} : Scalar channel capacity

C_{MISO} : MISO channel capacity

C_{SIMO} : SIMO channel capacity

d : Distance between the transmit and receive antennas,

E_b : Energy per bit

G : Generator matrix

G_t : Transmitter gain

G_r : Receiver gain

H : Channel coefficients matrix

H_t : Time-domain channel matrix

H^H: Hermitian transpose

$h(t)$: Impulse response

$h(\tau, t)$: Impulse response of the time-variant channel

$h_{j,i}$: Impulse responses of the channels from the i th transmit antenna to j th receive antenna.

$I_0(x)$: Modified Bessel function

I_{M_r} : $M_r \times M_r$ Identity matrix

i, j, k: Integers

J : Vector symbol

K_r : Rice factor

k_H: Rank of the channel matrix

$Mod(.)$: Modulation operation

M_r : Number of receiving antennas

M_t : Number of transmitting antennas

N_0 : Noise power spectral density

n_j : Noise samples

p_0 : ASCII code of the original watermark.

p_e : Encrypted watermark

P_r : Received power

P_t : Transmitted power

R_{xx} : Correlation matrix

r_s :   Spatial rate

$s_0, s_1, \ldots, s_K, s_{K+1}, \ldots, s_{N-1}$: Transmitted data symbols

s_{K+1}^*, s_K^* : Complex conjugates of s_{K+1}, s_K

$s(t)$: Received signal at time t

T_c : Coherence time

T_s : Symbol period (reciprocal bandwidth)

$tr(.)$: Trace of a matrix

$x(t)$: Transmitted signal

x_i : Transmitted symbols

$x^\wedge$: Transmitted vector symbols

y : Received vector

$\mathbb{Q}^{M_t}$: Entire set of possible vector symbols

λ : Wavelength of the carrier frequency

λ_i : Power gain

η_t : Time-domain additive white Gaussian noise vector.

Γ $(.)$: Gamma function

σ_τ : rms delay spread of the channel

σ : Standard deviation

σ^2 : Noise variance

$\propto_1, \propto_2$: Independent random variables with Rayleigh PDF.

$\theta_{1,}\ \theta_2$: Independent random variables with uniform PDF over $[0.2\pi]$

τ : Time delay

τ_{total} : Duration of the impulse response

$*$: Convolution operation

LIST OF ABBREVATIONS

AES	:	advanced encryption standard
ASCII	:	American Standard Code for Information Interchange
ASK	:	amplitude-shift keying
AWGN	:	additive white Gaussian noise
BER	:	bit-error-rate
BPSK	:	binary phase-shift keying
CDMA	:	Code Division Multiple Access
CSI	:	channel state information
CDF	:	cumulative distribution function
DCT	:	discrete cosine transforms
DWT	:	discrete wavelet transforms
EPR	:	electronic patient records
FDM	:	frequency division multiplexing
FDMA	:	frequency division multiple access
ICI	:	inter channel interference
i. i. d	:	independent and identically distributed
ISI	:	inter symbol interference
JPEG	:	joint photographic experts group
LDPC	:	low density parity check codes
LSB	:	least significant bit
LOS	:	line-of-sight
MATLAB	:	matrix laboratory

MFSK	:	minimum frequency shift keying
MIMO	:	multiple-input multiple-output
MISO	:	multiple-input single-output
ML	:	maximum likelihood
MMSE	:	minimum mean square error
MRC	:	maximal ratio combining
MRI	:	magnetic-resonance- imaging
OFDM	:	orthogonal frequency division multiplexing
OWDM	:	orthogonal wavelet division multiplexing
PAM	:	pulse amplitude modulation
PDF	:	probability density function
PSK	:	phase shift keying
P/S	:	parallel to serial conversion unit
QPSK	:	quadrature phase shift keying
QAM	:	quadrature amplitude modulation
RS	:	Reed Solomon
Rx	:	receiver
S/P	:	serial to parallel conversion unit
SNR	:	signal-to-noise ratio
SISO	:	single-input single-output
SIMO	:	single-input multiple-output
SDMA	:	space division multiple access
SDM	:	space division multiplexing
STBC	:	space-time block codes
STTC	:	space-time trellis codes

STFC	:	space-time frequency codes
SFBC	:	space frequency block coding
TDMA	:	Time Division Multiple Access
Tx	:	transmitter
V-BLAST	:	vertical-Bell laboratories layered space-time
ZF	:	zero forcing

CHAPTER 1

INTRODUCTION

1.1. Background and motivation

The rapid development of technologies and wireless communication systems has brought exponential growth in medical services to the community. Now a days, most of the hospitals are adapting to the technological development and providing most innovative support material and technical resources to the medical staff. The development of telemedicine or 'medicine at a range' has played a vital role in this massive technological breakthrough. The increased use of networks technology assures not only the health care delivery, but also the interconnection and exchange of medical databases between hospitals located at different geographical regions through a wireless network. Exchange of databases between hospitals requires efficient transmission and storage to cut down the health care cost. This exchange involves a large amount of critical patient information, such as text data and medical images. It requires large memory and causes transmission overheads when transmitted separately using information media like the internet. A feasible solution to save the storage and transmission overheads is to embed the text file as a watermark into the medical images. It combines the advantage of data security and efficient memory utilization. As such, recently more attention is being focused in the literature on embedding watermark into the medical images [1-2]. For greater security, the watermark is to be encrypted before embedding it into medical image of the patient [3]. For the purpose of robustness, the encrypted watermark is coded by the concatenation of Reed Solomon (RS) codes and low density parity check codes (LDPC) before embedding it into a medical image of the patient. Further, during medical image transmission, it is particularly essential to preserve all the

describing features of the image so that the diagnosis is error free. For this reason, the lossy techniques, which tend to produce high compression ratios, such as 1:10 and 1:30, are not acceptable in medical image compression [4]. Joint photographic experts group (JPEG) with discrete cosine transform (DCT) compression is optimized for visual perception and may be more visually correct. Hence, in order not to lose the critical information contained in the medical images, lossless JPEG (compression ratio. 1.6:1) is preferred [5]. However, even this low ratio compression may not be permissible on watermarked medical images to protect all the features of the image. Hence, it is necessary to transmit watermarked medical images without compression.

Multimedia communications through wireless channels are becoming more and more popular with the rapid development of wireless cellular systems and wireless local area networks. However, there are many challenges that still exist in developing an efficient wireless transmission system over hybrid wireless networks. Some of these challenges are caused by severe wireless channel conditions and some from resource limitations, such as power constraints and bandwidth. Compared to wire channels the capacity of wireless channels is much lower, and bit error rate is much higher due to severe wireless channel conditions, such as multipath fading, co-channel interference, and disturbances of noise. These wireless fluctuating channel characteristics are the greatest impediments for designing efficient transmission systems over wireless environments.

Operating in a time varying multipath fading environment is one of the biggest challenges under limited power constraints in wireless communications. The other challenge is the limited availability of the frequency spectrum. Future wireless systems will be required to support higher

data rates and reliable communication under spectrum limitation and multipath fading environment.

In order to improve the reliability without increasing the emitted power, time or frequency or space diversity can be exploited. In time diversity, the received signal can be sampled at a higher rate, thus providing more than one sample per transmitted symbol. In frequency diversity, the same signal can be transmitted over a number of carriers. Both these diversity techniques require a larger bandwidth. In space diversity, the same information can be transmitted or received through multiple antennas. Employing multiple antennas at the transmitter and the receiver aggrandizes the quality of a wireless communication without increasing the bandwidth and transmitted power. Recently, multiple-input multiple-output (MIMO) systems have been under active investigation in view of their providing a more reliable reception compared to that provided by a single-input single-output (SISO) system and because of the potential for achieving higher data rates.

Orthogonal frequency division multiplexing (OFDM) is a broadly-used method in broadband wireless communications. OFDM has been adopted by various wireless communication standards due to its effectiveness in multipath fading channels. Motivated by the huge demands for fast and reliable communications over wireless channels, future wireless communication systems should provide higher data rate, low complexity data processing, and robust performance. In practice, however, the wireless channel is typically non-line-of-sight channel, which has much impairment such as time-selective and frequency-selective fading. To overcome these impairments, one promising solution is to combine the two powerful technologies, MIMO and OFDM. The combination of OFDM and MIMO can achieve higher data rates and provide

high performance in very challenging channels that may be time-selective and frequency-selective. OFDM mitigates the fading effects and MIMO enhances the capacity and diversity.

1.2. Basic Wireless Communication System

The basic block diagram of a wireless communication system is shown in Figure 1.1. The various blocks are described below [6].
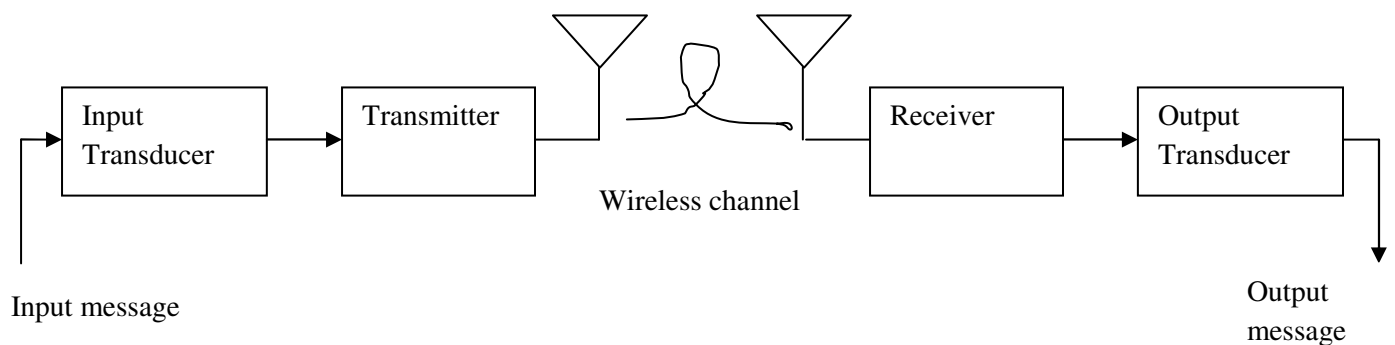
Fig. 1.1. Block diagram of a basic wireless communication system

Input transducer

The input message could be a human voice, an image or data. This input is converted by the input transducer into an electrical waveform, referred to as the baseband signal or message signal.

Transmitter

For efficient transmission, the transmitter modifies the baseband signal. The transmitter generally consists of one or more of the subsystems, such as a pre-emphasizer, a sampler, a quantizer, a coder and a modulator.

Channel

The channel is the medium between the transmitter and receiver, which could be a wire, a coaxial cable, an optical fiber or a free space etc., which carries the information from the transmitter to the receiver. Based on the type of channel, modern communication systems can be divided into two categories: wired communication systems and wireless communication systems.

Receiver

The receiver processes the signal received through the channel by undoing the signal modifications made at the transmitter and in the channel. The task of the receiver is to extract the message from the distorted and noisy signal at the channel output. The receiver may consist of a demodulator, a decoder, a filter, and a de-emphasizer.

Output transducer

The receiver output is fed to the output transducer, which converts the electrical signal to its original form. Transmitters and receivers should be carefully designed to overcome distortion and noise. The major goal of a physical layer communication system is to transmit information accurately and efficiently from the point of view of power and spectrum utilization.

1.3. Objectives of the Research

The main focus of this research is on developing different schemes for transmission of watermarked medical images over fading channels.

The first objective of the thesis is to develop a robust digital watermarking scheme. This scheme combines the advantages of memory utilization and data security. In this scheme, at the transmitter side, in order to prevent unauthorized access the data is first encrypted by encryption unit and then the encrypted information is coded by RS-LDPC codes for robustness. The spatial

domain digital watermarking technique is adapted to embed the encrypted and coded data as a watermark into the lower order bits of the image pixels. At the receiver side, the watermark extraction unit, RS-LDPC decoder, and decryption unit perform the reverse process to recover the original data. This scheme is used for digital watermarking in the transmission schemes proposed in this thesis.

The second objective of the thesis is to develop a robust scheme for watermarked medical image transmission over impulsive noisy wireless channels. Usually, wireless channels are affected by severe channel conditions such as fading and path loss. As such, wireless channels have high bit error rates and fluctuating characteristics. During image transmission over impulsive noisy wireless channels, the errant data must be recovered from the received signal. In this scheme, turbo channel coding is proposed to recover the errant data from the received signal.

The third objective of the thesis is to develop a MIMO scheme for watermarked medical image transmission over Rayleigh fading channels. Modern wireless services require high capacity and reliable channels. For the purpose of improving the channel capacity and reliability, a MIMO scheme is proposed. MIMO can improve the channel capacity as well as provide diversity gain. Maximum likelihood (ML) detection is proposed at the receiver side, which provides an efficient performance.

The fourth objective of the thesis is to develop a MIMO SFBC OFDM scheme for watermarked medical image transmission over Rayleigh fading channels. Usually, MIMO channels suffer from frequency selective fading. To mitigate the frequency selective fading or potential multipath fading in channels, a combination of MIMO and OFDM is proposed in this scheme. In order to enhance the bandwidth efficiency, space frequency block coding (SFBC) is employed.

For improving the performance of the system, V-BLAST based MMSE detection is proposed at the receiver side.

1.4. Organization of the Thesis

The following is a detailed outline of the remaining chapters of the thesis.

In Chapter 2, some preliminaries required for the development of different schemes for transmission of watermarked medical images over fading channels is described. First, the basic concepts of wireless channels, fading and fading channel statistical models are briefly reviewed. Then, MIMO communications, OFDM technique and MIMO-OFDM systems are briefly described.

In Chapter 3, a robust digital watermarking method is presented. First, basic concepts of the digital watermarking such as types of watermarks and types of watermarking methods are briefly discussed using functional blocks. The efficacy of the proposed scheme is illustrated through simulation results.

In Chapter 4, a robust scheme for watermarked medical image transmission over impulsive noisy channels is proposed. First, the basic building blocks (JPEG Compression, turbo coding) which are used in the proposed scheme are briefly reviewed. Then, the implementation of the proposed scheme is explained in detail. The performance proposed scheme is demonstrated through experimental results.

In Chapter 5, a scheme with a MIMO channel for transmission of watermarked medical images over Rayleigh fading channels is suggested. First, the basic building blocks (2x2, 4x4 MIMO channels, MIMO ML detectors) of the proposed scheme are explained in brief. Then, the

implementation of the proposed scheme is described. The proposed scheme is validated through experiments based on computer simulation using the bit-error-rate (BER) as the performance measure.

In Chapter 6, a MIMO SFBC OFDM scheme for transmission of watermarked medical images over Rayleigh fading channels is developed. First, the basic building blocks (V-BLAST, MMSE) of the proposed scheme are briefly explained and then the proposed MIMO SFBC OFDM system design is discussed. Next, the implementation of the proposed scheme is explained in detail. A number of experiments based on computer simulation are conducted to illustrate the effectiveness of the proposed scheme.

In Chapter 7, a comparison of the three proposed schemes for watermarked medical image transmission over wireless channels is presented.

Finally, Chapter 8 draws some conclusions on the work contained in the thesis and suggests some proposals and ideas for future research work.

CHAPTER 2

PRELIMINARIES

This chapter introduces some basic concepts and principles involved in the development of different schemes for transmission of watermarked medical images over fading channels. Some state of the art literature relating to the proposed work is also reviewed, thus providing necessary background material for the development of the work proposed in the later chapters.

2.1. Wireless channel

Due to various transmission impairments normally present in any communication system, the received signal differs from the transmitted signal. These impairments introduce different random modifications to the original signal, thus degrading the signal quality. Some of the important transmission impairments are discussed below [7].

Attenuation

During signal transmission from the source to the destination the energy and amplitude of the signal is reduced due to absorption or scattering of photons. This is called attenuation. It increases with transmission distance over any transmission medium, and varies as a function of the frequency; it is greater at higher frequencies. A relay could be used between the transmitter and the receiver to compensate the attenuation.

Noise

Noise is the unwanted signal which is received at the receiver along with the transmitted signal. It is the most limiting factor in the performance of a communication system. There are many sources for noise and some of these are listed below.

- **Thermal noise:** This is produced due to the thermal agitation in electronic components. It places an upper bound on the performance of a communication system, same it is present in all electronic devices and cannot be eliminated. It has a uniform frequency spectrum distribution and therefore referred to as white noise.

- **Crosstalk noise:** Crosstalk can occur when an unwanted signal is picked up by antenna.

- **Impulse noise:** It consists of noise spikes or irregular pulses of short duration but of high amplitude. It is generated form electromagnetic disturbance such as lightening.

Free space loss

Due to the signal spread in space, the signal disperses with distance. Free space loss is the loss in the signal strength that results from a line-of-sight (LOS) path through free space. Free space loss is proportional to the square of the distance between the transmitter and the receiver.

The propagation loss from the transmit antenna to the receive antenna in free space can be derived by the Friis power transmission equation [8]

$$P_r(d) \approx P_t G_t G_r \left(\frac{\lambda}{4\pi d}\right)^2, \tag{2.1}$$

where d is the distance between the transmit and receive antennas, λ is the wavelength of the carrier frequency, P_r, P_t are the received and transmitted power, G_t and G_r are the gains of the transmit and receive antennas, respectively.

Multipath

For wireless transmission between a transmitter and a receiver, there could be a direct line of sight between them, which happens when there are no obstacles in the signal path. But when there are obstacles, the signal may be reflected by such obstacles, and hence multiple copies of the signal with varying delays can be received.

2.2. Fading

Basically, fading can be classified as two types: large-scale fading and small-scale fading. These are briefly described in the following subsections.

Large-scale fading

This is due to loss of the signal as a function of distance and shadowing by large objects such as building and hells. This happens when the mobile moves through a distance which is of the order of a cell. It is independent of the frequency.

Small-scale fading

Small scale fading or fading is used to describe the rapid fluctuations of the phases, amplitudes, or multipath delays of a radio wave over a short time period or travel distance, so that large scale fading or large scale path loss effects may be not considered. Fading in a mobile environment is one of the most challenging technical problems facing communication system engineers. For most practical wireless communication channels, fading is the most important factor to be considered when describing the channel and predicting the system performance. These subsections address the factors influencing small-scale fading or fading, types of fading.

2.2.1. Factors influencing small-scale fading

A number of physical factors in signal propagation channel influence fading. These include:

Multipath propagation: The presence of scatters and reflecting objects in the channel creates constantly varying environment for electromagnetic wave. Such a random variations results in multiple versions of the transmitted signal received at the receiver. The random amplitude and phase of the different multipath components cause fluctuations in signal strength. This type of fluctuations in signal strength induces fading and signal distortion.

Speed of the mobile: The relative motion between the mobile receiver and base station results in random frequency modulation due to different Doppler shifts on each of the multipath components. Doppler shift will be negative or positive depending on whether the mobile receiver is moving towards or away from the base station.

Speed of surrounding objects: If objects in the radio channel are in motion, then they produce a time varying Doppler shift on multipath components. If the surrounding objects move at a rate greater than that of the mobile, then this effect dominates the fading.

The transmission bandwidth of the signal: If the bandwidth of channel is less than the bandwidth of the transmitted signal, then the received signal will be distorted. The bandwidth of the channel is quantified by the coherence bandwidth which is related to the multipath structure of the channel. The coherence bandwidth is a figure of merit of the system and a measure of the maximum frequency difference for which signals are correlated in amplitude. If the multipath channel has a large bandwidth compared to the transmitted signal, the amplitude of the signal will vary rapidly, but the signal cannot be distorted in time.

2.2.2. Types of small-scale fading

Depending on the relation between the channel parameters (such as Doppler spread and delay spread) and the signal parameters (such as symbol period, bandwidth, etc.), different types of fading will occur. Doppler spread leads to time-selective fading and frequency dispersion. Multipath delay spread leads to time dispersion and frequency-selective fading [8].

(i) Fading effects due to Doppler spread

Slow fading

Slow fading represents the average signal power attenuation or path loss due to transmission over a long distance or a large area. As the environment varies over long distance, slow fading is caused by forests, mountains, clumps of buildings, etc that may exist between the transmitter and the receiver. In a slow fading channel, the impulse response of the channel varies at a rate much slower than the transmitted base band signal. That is, the coherence time of the signal is longer than the symbol duration time of the transmitted signal. In the frequency domain, the Doppler spread of the channel is much less than the bandwidth of the baseband signals. Therefore, slow fading occurs if

$$T_s \ll T_c \quad \text{and} \quad B_s \gg B_D \tag{2.2}$$

where T_s is the symbol period (reciprocal bandwidth), B_s is the bandwidth of the transmitted signal, T_c is the coherence time, and B_D is the Doppler spread of the channel .

Fast fading

In a fast fading channel, the impulse response of the channel rapidly changes within the symbol duration. That is, the coherence time of the signal is smaller than the symbol duration time of the

13

transmitted signal. Due to Doppler spread, frequency dispersion (also called time selective fading) is caused, leading to signal distortion. In the frequency domain, due to fast fading, signal distortion increases with the increasing Doppler spread relative to the transmitted signal bandwidth. Therefore, fast fading occurs if

$$T_s > T_c \quad \text{and} \quad B_s < B_D \tag{2.3}$$

(ii) Fading effects due to multipath time delay spread

Flat fading

In a flat fading channel, the channel has a linear phase response and a constant gain over a bandwidth which is larger than the bandwidth of the transmitted signal. This is the most common type of fading in wireless communications. In this type of fading, the multipath structure of the channel is such that the spectral characteristics of the transmitted signal are conserved at the receiver. However, the strength of the received signal varies with time, due to the variations in the gain of the channel caused by multipath. In a flat fading channel, the symbol period of the transmitted signal is much greater than the multipath time delay spread of the channel. Flat fading channels are also called as amplitude varying channels. Sometimes these channels are also referred to as narrow band channels. To summarize, flat fading occurs if

$$B_s \ll B_c \text{ and } T_s \gg \sigma_\tau \tag{2.4}$$

where $B_c \ and \ \sigma_\tau$ are the coherence bandwidth and rms delay spread of the channel .

Frequency selective fading

In a frequency selective fading channel, the channel has a linear phase response and a constant gain over a bandwidth which is less than the bandwidth of the transmitted signal. Under such

conditions, the impulse response of the channel has a multipath delay spread which is greater than the symbol period of the transmitted message signal. When this occurs, multiple versions of the transmitted signal are received at the receiving antenna and hence, the received signal gets distorted. This type of frequency selective fading channel is also called as a wideband channel, since the bandwidth of the transmitted signal is wider than the bandwidth of the impulse response of the channel. To summarize, frequency selective fading occurs if

$$B_s > B_c \text{ and } T_s < \sigma_\tau \qquad (2.5)$$

2.3. Multipath fading

As mentioned earlier, in a wireless mobile system, a signal can travel from the transmitter to the receiver through multiple paths. Multipath propagation causes fluctuation in the amplitude, phase and angle of arrival of the signal creating multipath fading. Four basic propagation mechanisms play a role in multipath fading: reflection, refraction, diffraction and scattering. Reflection and refraction occur when a propagating electromagnetic signal impinges on an object that has large dimensions compared to the wavelength of the propagating signal. Diffraction occurs when the radio wave path is obstructed by a surface that has sharp edges. Finally, Scattering occurs when the propagating radio wave goes through a medium composed of many small objects (in terms of wavelength).

2.4. Channel fading

When designing a communication system, a communication engineer has to consider all the factors which may affect the propagation of the signal; hence he needs to estimate the effects of

noise and multipath fading on the mobile channel. Some typical fading channels are discussed below.

Additive white Gaussian noise (AWGN) channel

In such a channel, the thermal noise is only impairment which is encountered for the propagation of the transmitted signal. This noise may be associated with the physical channel itself, as well as with the electronics at or between the transmitter and the receiver. In an AWGN channel, the signal is degraded by white noise, which has a constant spectral density and a Gaussian distribution of amplitude.

Rayleigh fading

Rayleigh fading occurs when there are multiple indirect paths between the transmitter and the receiver and no direct non-fading or line-of sight (LOS) path. It represents the worst case scenario for the transmission channel. Rayleigh fading assumes that a received multipath signal consists of a large number of reflected waves with independent and identically distributed phase and amplitude. The envelope of the received carrier signal is Rayleigh distributed in wireless communications [9]. The Rayleigh distribution has a PDF given by

$$p(r) \quad = \quad \frac{r}{\sigma^2} e^{-\frac{r^2}{2\sigma^2}} \quad 0 \leq r \leq \infty \tag{2.6}$$

$$0 \qquad\qquad r < 0$$

$$p_{r^2}(r) = \quad \frac{1}{2\sigma^2} e^{-\frac{r}{2\sigma^2}} \tag{2.7}$$

where $\sigma^2 = E[r^2]/2$ is the total power in the received signal and σ is the standard deviation.

The cumulative distribution function (CDF) is given by

$$P(R) = P_r(\text{r} \leq R) = 1 - e^{-\frac{R^2}{2\sigma^2}} \tag{2.8}$$

The mean of r is $E[r] = \sigma\sqrt{\frac{\pi}{2}}$, and the root-mean-squared (rms) value of the distribution is

$E[\sqrt{r^2}] = \sqrt{2}\sigma$. The pdf has it maximum at $r = \sigma$ with its mean value at $E[r] = \sigma\sqrt{\frac{\pi}{2}}$ and has

variance of $0.429\ \sigma^2$.

The multipath model is commonly modeled as a two-ray model for illustrating Rayleigh fading.

The impulse response is given by

$$h(t) = \propto_1 e^{j\theta_1(t)}\delta(t) + \propto_1 e^{j\theta_2(t)}\delta(t - \tau) \tag{2.9}$$

where

$\propto_1, \propto_2$ are independent random variables with Rayleigh PDF.

$\theta_1,\ \theta_2$ are independent random variables with uniform PDF over $[0.2\pi]$, and

τ is the time delay.

Ricean fading

Ricean fading best describes a situation where a dominant non-fading, line-of-sight (LOS), component is present in addition to a number of indirect multipath signals. The fading envelope of this model is described by Ricean probability density function (PDF). Additive white Gaussian noise and Ricean channels provide fairly good performance corresponding to an open country environment, while Rayleigh channel, which best describes urban environment fading,

provides relatively worse performance. Line-of-sight path is introduced into the Rayleigh fading environment, the fading turns into Rice-distributed fading. It is also a small scale fading.

The Ricean distribution is given by

$$p(r) \quad = \quad \frac{r}{\sigma^2} e^{-\frac{(r^2+A^2)}{2\sigma^2}} I_0\left(\frac{Ar}{\sigma^2}\right) \quad (A \geq 0, r \geq 0) \tag{2.10}$$

$$0 \qquad\qquad r < 0$$

where $I_0(x)$ is the modified Bessel function of the first kind and zero order, $K_r = \frac{Ar}{\sigma^2}$ is the rice factor.

Nakagami fading

The Nakagami model is another very popular empirical fading model [9]

$$p(r) = \frac{2}{\Gamma(m)} \left(\frac{m}{2\sigma^2}\right)^m r^{2m-1} e^{-m\frac{r^2}{2\sigma^2}} \tag{2.11}$$

where

$$\sigma^2 = \frac{1}{2} E[r^2], \ \Gamma(.) \text{ is the gamma function}$$

$$m \geq \frac{1}{2} \text{ is the fading figure.}$$

The received instantaneous power satisfies a gamma distribution. The phase of the signal is uniformly distributed in [0, 2π). The Nakagami distribution is a general model obtained from experimental data fitting and its shape is very similar to that of the Rice distribution. The shape parameter 'm' measures the severity of fading. When $m = 1$, it corresponds to Rayleigh fading,

when $m \to \infty$, it corresponds to AWGN channel (that is, there is no fading), and when $m > 1$ the Nakagami fading is close to Ricean fading.

However, due to lack of physical basis, the Nakagami distribution is not as popular as the Ricean and Rayleigh fading models in mobile communications. Many other fading channel models are discussed in [10].

2.5. MIMO Communications

In multiple-input multiple-output (MIMO) communications, the system is equipped with multiple antennas at both the transmitter and the receiver. Multiple antenna system gives a more reliable performance through array gain, diversity and spatial multiplexing. These concepts are briefly discussed below [11, 12].

2.5.1. Array gain

In MIMO communications, array gain is the average increase in the SNR at the receiver that occurs from the coherent combining effect of the multiple antennas at the transmitter or receiver or both. Usually, multi antenna systems require a perfect knowledge of the channel either at the receiver or the transmitter or both to achieve an array gain.

Transmitter array gain: If the channel is known to the transmitter with multiple antennas, the transmitter will weigh the transmission with weights, depending on the channel coefficients, so that there is coherent combining at one antenna receiver. This is the MISO case. This type of array gain is called transmitter array gain.

Receiver array gain: If we have a single antenna at the transmitter and no knowledge of the channel and a receiver with multiple antennas, which has perfect knowledge of the channel, then

the receiver can suitably weight the incoming signals so that they coherently add up at the output, thereby enhancing the signal. This is the SIMO case. This type of array gain is called receiver array gain.

2.5.2. Diversity gain

Due to the detrimental effect of multipath fading, the signal transmission over broadband wireless channels always suffers from attenuation, and this can severely degrade the reception performance. In MIMO systems, the same information is transmitted from multiple transmit antennas and simultaneously received at multiple receive antennas. Since the fading for each link between a pair of transmit and receive antennas usually can be considered to be independent, the probability that the information is detected exactly is increased [11]. Apart from the spatial diversity, other forms of diversities exist: temporal diversity and frequency diversity. In temporal and frequency domains, replicas of the faded signals are received in the form of redundancy. The MIMO system achieves diversity through repetition coding that carries the same information symbol at different time slots from different transmit antennas. Space time (ST) coding is a more bandwidth efficient coding scheme [13], which transmits a block of information symbols in different orders from the different antennas.

2.5.3. Spatial multiplexing

The capacity of a MIMO system is much higher than that of a single-antenna system. The channel capacity can be linearly increased in proportion to the number of antennas. MIMO systems provide more spatial freedom or spatial multiplexing, so that different information can be transmitted over multiple antennas simultaneously, thereby enhancing the system throughput.

At the receiver, spatial multiplexing needs a dedicated detection algorithm to sort out the different transmitted signals from the mixed one.

2.5.4. Multi antenna Systems

Multi antenna systems can be classified as single-input multiple-output (SIMO), multiple-input single-output (MISO), and multiple-input multiple-output (MIMO) systems.

In order to develop the input-output relations of SIMO, MISO, MIMO systems, we first describe the single-input single-output (SISO) system [14].

(i) Single-Input Single-Output System

The schematic block diagram of a SISO system is depicted in Figure 2.1.
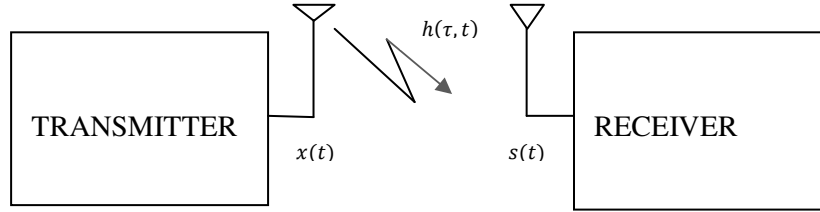
Fig. 2.1. Block diagram of a SISO system

In this figure, $h(\tau, t)$ is the impulse response of the time-variant channel from the transmitter to the receiver.

The input-output relationship of the SISO system is given by

$$s(t) = \int_0^{\tau_{total}} h(\tau, t)x(t - \tau)d\tau = h(\tau, t) * x(t) \qquad (2.12)$$

where $x(t)$ is the transmitted signal, $s(t)$ is the received signal at time t, τ_{total} is the duration of the impulse response, and $*$ denotes the convolution operation.

(ii) Single-Input Multiple-Output System

The schematic block diagram of a SIMO system with single transmit antenna and M_r receive antennas is depicted in Figure 2.2.
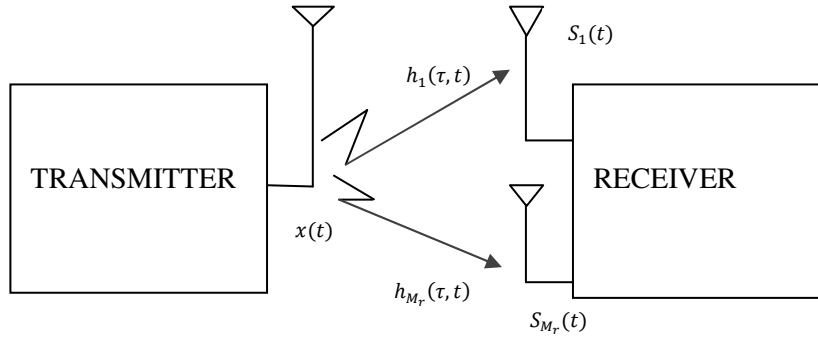
Fig. 2.2. Block diagram of a SIMO system

The impulse responses from the transmit antenna to the M_r receive antennas are represented by $h_i(\tau, t)$ where $i = 1, 2, 3, \dots \dots, M_r$

The received signals at the respective receive antennas are given by

$$S_1(t) = h_1(\tau, t) * x(t) \tag{2.13}$$

$$S_2(t) = h_2(\tau, t) * x(t)$$

$$.$$

$$S_{M_r}(t) = h_{M_r}(\tau, t) * x(t) \tag{2.14}$$

Therefore, the input-output relationship of a SIMO system can be expressed as

$$S(t) = h(\tau, t) * x(t) \tag{2.15}$$

where

$$S(t) = [\ S_1(t)\ \ S_2(t) \dots \dots \dots \dots \dots S_{M_r}(t)]^{\ T} \text{ is the received signal vector}$$

$$h(t) = [\ h_1(t)\ \ h_2(t) \dots \dots \dots \dots \dots h_{M_r}(t)]^{\ T} \text{ is the channel vector.}$$

(iii) Multiple-Input Single-Output System

The schematic block diagram of a MISO system with M_t transmit antennas and a single receive antenna is depicted in Figure 2.3.
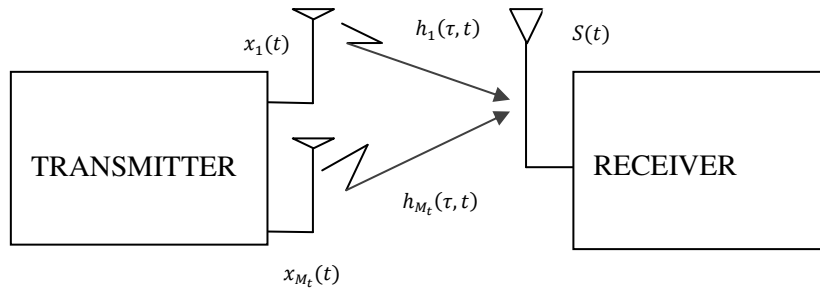
Fig.2.3. Block diagram of a MISO system

The multiple-transmitted signals $x_i(t)$, $i = 1, 2, \dots \dots \dots M_t$ are convolved with $h_i(\tau, t), i = 1, 2, \dots \dots \dots M_t$. A superposition of the multi-antenna transmissions through the channel is received at the receiving antenna. The received signal can be expressed as

$$S(t) = x_1(t) * h_1(\tau, t) + x_2(t) * h_2(\tau, t) \dots \dots + x_{M_t}(t) * h_{M_t}(\tau, t) \tag{2.16}$$

We can express the input-output relationship of the MISO system as

$$S(t) = h(\tau, t) * x(t) \tag{2.17}$$

where

$$x(t) = [\, x_1(t)\ \ x_2(t) \ldots \ldots \ldots \ldots . x_{M_t}(t)]^{\,T}$$ is the transmission vector.

$$h(t) = [\, h_1(t)\ \ h_2(t) \ldots \ldots \ldots \ldots . h_{M_r}(t)]^{\,T}$$ is the channel vector.

(iv) MIMO system

The schematic block diagram of a MIMO system with M_t transmit antennas and M_r receive antennas is depicted in Figure 2.4.
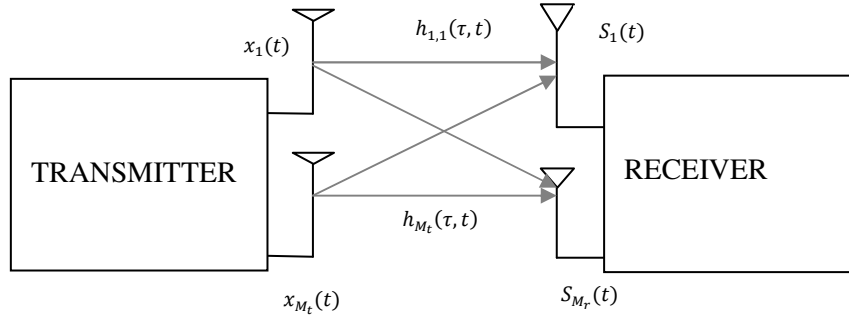
Fig.2.4. Block diagram of MIMO system

The received signal at the first receiving antenna is given by

$$S_1(t) = x_1(t) * h_{1,1}(\tau, t) + x_2(t) * h_{2,1}(\tau, t) \ldots \ldots . + x_{M_t}(t) * h_{1,M_t}(\tau, t) \qquad (2.18)$$

The received signal at the last receiving antenna is given by

$$S_{M_r}(t) = x_1(t) * h_{M_r,1}(\tau, t) + x_2(t) * h_{2,1}(\tau, t) \ldots \ldots . + x_{M_t}(t) * h_{M_r,M_t}(\tau, t) \qquad (2.19)$$

Representing the signals at the transmitter antennas in a vector form, the $M_t \times 1$ transmission vector is

$$x(t) = [\, x_1(t)\ \ x_2(t) \ldots \ldots \ldots \ldots . x_{M_t}(t)]^{\,T}$$

The signals at the receiver antennas may be expressed in a vector form as

$$S(t) = [\, S_1(t) \; S_2(t) \,\ldots\ldots\ldots\ldots\ldots.S_{M_r}(t)]^{\,T}$$

The input-output relationship for the MIMO system is given by

$$S(t) = H(\tau, t) * x(t) \tag{2.20}$$

where $H(\tau, t)$ is the $M_r \times M_t$ channel matrix given by

$$H(\tau, t) = \begin{bmatrix} h_{1,1}(\tau, t) & h_{1,2}(\tau, t) & . & . & . & h_{1,M_t}(\tau, t) \\ . & . & . & . & & . \\ . & . & . & . & & . \\ h_{M_r,1}(\tau, t) & h_{M_r,2}(\tau, t) & . & . & . & h_{M_r,M_t}(\tau, t) \end{bmatrix} \tag{2.21}$$

2.5.5. MIMO channel

Consider a wireless communication system in which the transmitter contains M_t antennas and the receiver possesses M_r antennas.

Let us consider a $M_r \times M_t$ MIMO channel. The received signal for the $M_r \times M_t$ MIMO channel can be expressed as

$$y_j = \sum_{i=1}^{M_t} h_{j.i} x_i + n_j \tag{2.22}$$

where $h_{j.i}$ (i=1, 2...... M_t; j=1, 2........ M_r.) are independent and identically distributed (i.i.d) complex random variables representing the channel coefficient from the *ith* transmitter antenna to the *jth* receiver antenna, x_i (i=1, 2...... M_t) are the transmitted symbols, and n_j (j=1, 2..... M_r) are noise samples, which are i.i.d complex AWGN variables. Now, (2.22) can be represented in matrix form as

$$\begin{bmatrix} y_1 \\ y_2 \\ . \\ y_{M_r} \end{bmatrix} = \begin{bmatrix} h_{1,1} & . & h_{1,M_t} \\ h_{2,1} & . & h_{2,M_t} \\ . & . & . \\ . & . & . \\ h_{M_r,1} & . & h_{M_r,M_t} \end{bmatrix} \begin{bmatrix} x_1 \\ x_2 \\ . \\ x_{M_t} \end{bmatrix} + \begin{bmatrix} n_1 \\ n_2 \\ . \\ n_{M_r} \end{bmatrix} \qquad (2.23)$$

Equivalently, $\qquad\qquad\qquad\qquad y = \mathrm{H}x + n \qquad\qquad\qquad\qquad$ (2.24)

2.5.6. Capacity of a MIMO channel

We can write the expression for the capacity for a MIMO channel as [9]

$$C = \max_{tr(R_{xx})=M_t} log_2 \, det \left\{ I_{M_r} + \frac{SNR}{M_t} \mathrm{H} R_{xx} \mathrm{H}^H \right\} \qquad (2.25)$$

where I_{M_r} is the $M_r \times M_r$ identity matrix, SNR is the mean signal-to-noise ratio of each receiver branch, H^H is the Hermitian transpose of a channel matrix H, $tr(.)$ is the trace of a matrix and $R_{xx} = E[xx^H]$ is the correlation matrix of the transmit data.

When the channel state information is not available to the transmitter, we can assume equal power distribution among the transmitters, in which case R_{xx} is an identity matrix and (2.25) becomes

$$C = log_2 det \left\{ I_{M_r} + \frac{SNR}{M_t} \mathrm{HH}^H \right\} \qquad (2.26)$$

This is the capacity equation for MIMO channels with equal power. The optimization of this expression depends on whether or not the channel state information (CSI), namely, the H matrix is known to the transmitter.

No CSI at the transmitter

When there is full CSI at the receiver but no CSI at the transmitter, the capacity for MIMO channel has been already discussed and is given by equation (2.26):

$$C = log_2 det\left\{I_{M_r} + \frac{SNR}{M_t} HH^H\right\}$$

$$= \sum_{i=1}^{k_H} log_2\left\{1 + \frac{SNR}{M_t}\lambda_i\right\} \tag{2.27}$$

where k_H is the rank of H. Thus, the capacity of the MIMO channel is expressed as the sum of the capacities of k_H SISO channels, each having a power gain λ_i.

Case 1: SIMO: $M_t = 1$ and $M_r > 1$

In this case, $\lambda = M_r$ and

$$C_{SIMO} = log_2\{1 + SNR\ M_r\} > C_{AWGN} \tag{2.28}$$

where C_{AWGN} is the scalar channel capacity. The CSI at the transmitter does not show any impact on the SIMO channel capacity.

Case 2: MISO: $M_r = 1$ and $M_t > 1$ $\tag{2.29}$

In this case, $\lambda = M_t$ and

$$C_{MISO} = log_2\{1 + SNR\} = C_{AWGN} \tag{2.30}$$

The reason for the capacity of the SIMO channel to be greater than that of the MISO channel is that the transmitter in the MISO case cannot exploit the antenna array gain since it has no CSI.

Case 3: M_t large and $M_r > 1$

Applying the strong law of large number leads to

$$\frac{1}{M_t}HH^H \rightarrow M_r I_{M_r} \tag{2.31}$$

Thus

$$C \approx M_r log_2\{I_{M_r} + SNR\} = M_r \, C_{AWGN} \tag{2.32}$$

The capacity is M_r times to the scalar channel capacity.

CSI known to the transmitter

Consider a MIMO channel where the CSI is known at the both transmitter and the receiver. The water-filling principle or water-pouring principle can be derived by maximizing the channel capacity under the rule that less power is allocated to the channel that is in bad condition and more power allocated to the good channels. The complete analysis is given in [15].

The channel capacity is given by [9]

$$C = \max_{\sum_{i=1}^{k_H} \gamma_i} \sum_{i=1}^{k_H} log_2 \left\{ 1 + \frac{SNR}{M_t} \lambda_i \right\} \tag{2.33}$$

where $\gamma_i = E[|x_i|^2]$, and $k_H = \min [M_t, M_r]$.

2.6. Space-Time Coding

Space -time coding is specially designed for use with multiple transmit antennas. Space- time codes provide coding and diversity gain without sacrificing the bandwidth. Space-time coding is illustrated in Figure 2.5.
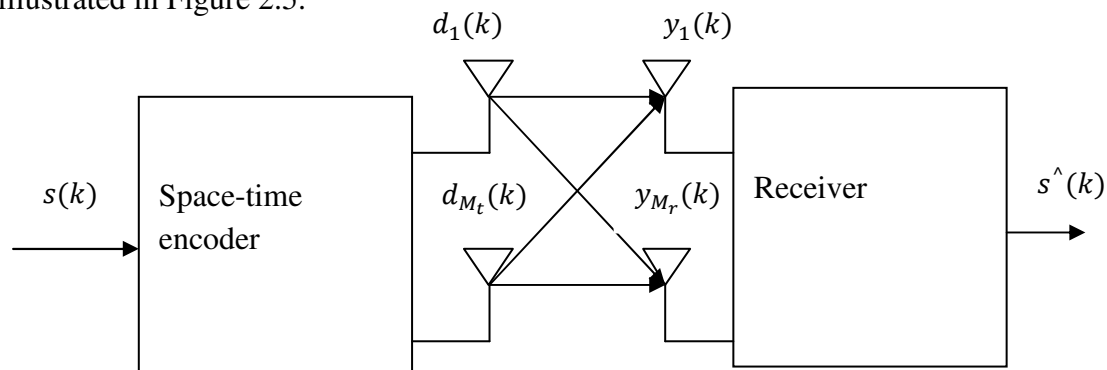
Fig. 2.5. Space-time coding system

The data symbol $s(k)$ is encoded into M_t code symbols $d_1(k), d_2(k), \ldots, d_{M_t}(k)$, each coded symbol being transmitted from different antennas simultaneously. The M_t code symbols are encoded in such a way that both the diversity gain and the coding gain are maximized at the receiver. Space-time coding ameliorates redundancy over space and time, since each antenna transmits the same, but differently encoded symbol. Thus, space-time coding maximizes the diversity gain. Space-time codes can be classified as space-time block codes (STBC) and space-time trellis codes (STTC). For space-time codes such as STBC and STTC, which achieve full diversity order, the spatial rate $r_s \leq 1$.

2.6.1. Space-time block code

(a) Alamouti code

The very first and well-known space time block code (STBC) is the Alamouti code [14]. In the Alamouti encoder, two consecutive symbols s_1 and s_2 are encoded with the following space-time codeword matrix:

$$S = \begin{bmatrix} s_1 & -s_2^* \\ s_2 & s_1^* \end{bmatrix} \tag{2.34}$$

This indicates that, during the first time slot, the first antenna transmits s_1 and the second antenna transmits s_2, respectively. During the next time slot, the first antenna transmits $-s_2^*$, and the second antenna transmits s_1^*, s_2^* and s_1^* being the complex conjugates of s_2 and s_1, respectively. It is the only STBC that can achieve its full diversity gain without sacrificing its data rate. The code rate is 1 because it takes two time-slots to transmit two symbols.

(b) 2-transmit, 1-receive Alamouti STBC coding

Fig. 2.6. Alamouti scheme with two transmit and one receive antennas

The Alamouti scheme with two transmit and one receive antennas is shown in Figure 2.6. From antennas 1 and 2, during the first symbol period two consecutive symbols $-s_2^*$ and s_1^* are transmitted simultaneously at time t. During the next symbol period symbols s_1 and s_2 are transmitted at time $t + T$. If y_1 and y_2, denote the signals received at the first and second time slots, respectively, then we have

$$[y_1 \quad y_2] = [h_1 \quad h_2] \begin{bmatrix} s_1 & -s_2^* \\ s_2 & s_1^* \end{bmatrix} + [\eta_1 \quad \eta_2] \tag{2.34}$$

$$= [h_1 s_1 + h_2 s_2 + \eta_1 \quad -h_1 s_2^* + h_2 s_1^* + \eta_2] \tag{2.35}$$

where h_1 is the channel impulse response from 1st transmit antenna to receive antenna, h_2 is the channel impulse response from 2nd transmit antenna to receive antenna, and η_1 and η_2 are the noise at time slots 1 and 2, respectively.

The received signals are computed by [14]

$$\tilde{s}_1 = h_1^* y_1 + h_2 y_2^* \tag{2.36}$$

and

$$\tilde{s}_2 = h_2^* y_1 - h_1 y_2^* \tag{2.37}$$

To decode, the ML decoder minimizes the following decision metric (for decoding) s_1 and s_2, respectively [12].

$$|\tilde{s}_1 - s_1|^2 + \xi|s_1|^2 \tag{2.38}$$

$$|\tilde{s}_2 - s_2|^2 + \xi|s_2|^2 \tag{2.39}$$

where

$$\xi = \left(-1 + \sum_{i=1}^{N_t} |h_i|^2\right) \tag{2.40}$$

2.6.2. BER with Alamouti (2x1) STBC

The bit error rate (BER) for a 2 branch maximal ratio combining (MRC), i.e., with one transmitting and two receiving antennas with BPSK modulation can be expressed as [16]

$$BER_{MRC(1x2)} = p_{MRC}^2 [1 + 2(1 - p_{MRC})] \tag{2.41}$$

where

$$p_{MRC} = \frac{1}{2} - \frac{1}{2}\left(1 + \frac{1}{E_b/N_0}\right)^{-1/2} \tag{2.42}$$

where E_b is the energy per bit and N_0 is the noise power spectral density.

It can be shown [13] that the performance of the Alamouti scheme with two transmitters and a single receiver is identical to that of the two-branch MRC provided that each transmit antenna in the Alamouti scheme radiates the same energy as the single transmit antenna for MRC. Then the BER for the Alamouti 2 transmit and 1 receive antenna STBC case with BPSK modulation can be written as

$$BER_{Alamouti(2x1)} = p_{Alamouti}^2[1 + 2(1 - p_{Alamouti})]$$
(2.43)

where

$$p_{Alamouti} = \frac{1}{2} - \frac{1}{2}\left(1 + \frac{2}{E_b/N_0}\right)^{-1/2}$$
(2.44)

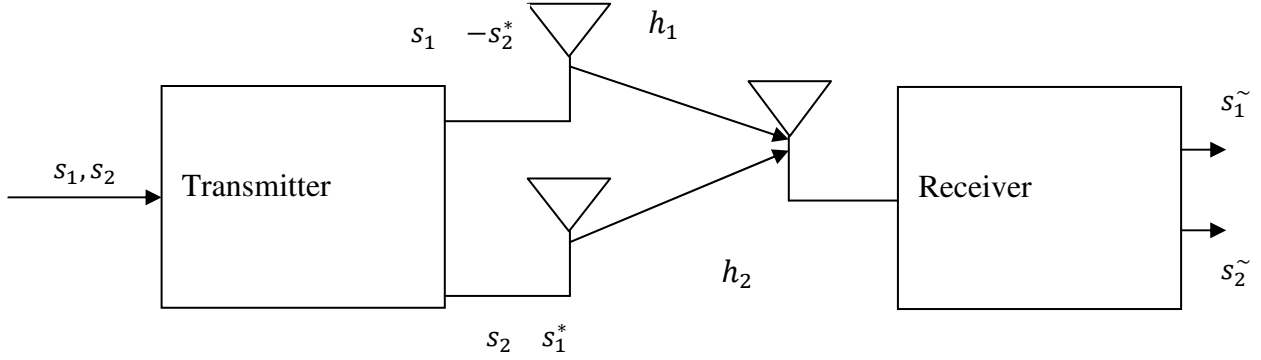### 2.6.3. 2-transmit, 2-receive Alamouti STBC coding
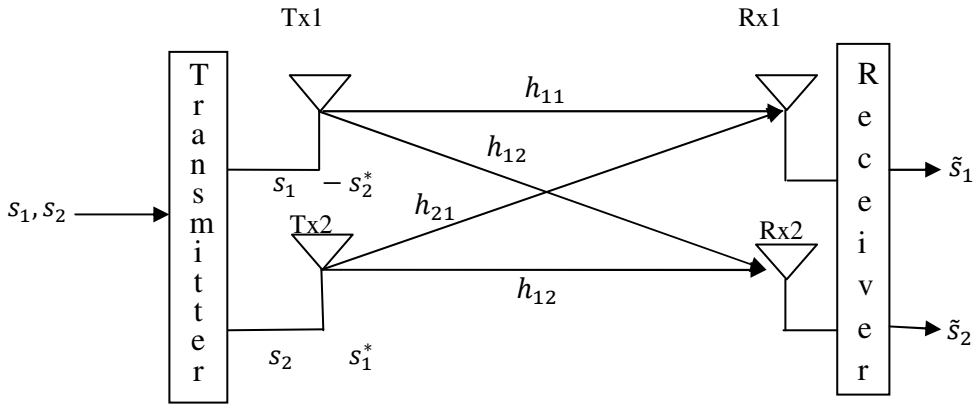
Fig. 2.7. Alamouti scheme with two transmit and two receive antennas

For the Alamouti scheme with two transmit and two receive antennas shown in Figure 2.7, if $y_{11}, y_{12}, y_{21}, y_{22}$,denote the signals received by antenna 1 at first time slot, by antenna 1 at second time slot, by antenna 2 at first time slot, by antenna 2 at second time slot, respectively, then we have

$$\begin{bmatrix} y_{11} & y_{12} \\ y_{21} & y_{22} \end{bmatrix} = \begin{bmatrix} h_{11} & h_{12} \\ h_{21} & h_{22} \end{bmatrix} \begin{bmatrix} s_1 & -s_2^* \\ s_2 & s_1^* \end{bmatrix} + \begin{bmatrix} \eta_{11} & \eta_{12} \\ \eta_{21} & \eta_{22} \end{bmatrix}$$
(2.45)

$$= \begin{bmatrix} h_{11}s_1 + h_{12}s_2 + \eta_{11} & -h_{11}s_2^* + h_{12}s_1^* + \eta_{21} \\ h_{21}s_1 + h_{22}s_2 + \eta_{21} & -h_{21}s_2^* + h_{22}s_1^* + \eta_{22} \end{bmatrix}$$
(2.46)

where h_{ij} is the channel impulse response from i^{th} receive antenna to, j^{th} transmit antenna, s_1, s_2 are the transmitted symbols, η_{11} and η_{12} are the noises at time slot 1 on receive antennas 1 and 2 respectively, and η_{21} and η_{22} are the noises at time slot 2 on receive antenna 1 and 2 respectively.

The received signals are given by [14]

$$\tilde{s}_1 = h_{11}^* y_{11} + h_{12} y_{12}^* + h_{21}^* y_{21} + h_{22} y_{22}^* \tag{2.47}$$

and

$$\tilde{s}_2 = h_{12}^* y_{11} - h_{11} y_{12}^* + h_{22}^* y_{21} - h_{22} y_{22}^* \tag{2.48}$$

To decode, the ML decoder minimizes the following decision metric (for decoding) s_1 and s_2, respectively [12].

$$|\tilde{s}_1 - s_1|^2 + \xi |s_1|^2 \tag{2.49}$$

$$|\tilde{s}_2 - s_2|^2 + \xi |s_2|^2 \tag{2.50}$$

where

$$\xi = \left(-1 + \sum_{i=1}^{N_r} \sum_{j=1}^{N_t} |h_{i,j}|^2 \right) \tag{2.51}$$

2.6.4. BER with Alamouti (2x2) STBC

The BER for a 4 branch MRC (i.e. with one transmitting and four receiving antennas) with BPSK modulation can be expressed as [16]

$$BER_{MRC(1x4)} = p_{MRC}^4 [1 + 4(1 - p_{MRC}) + 10(1 - p_{MRC})^2 + 20(1 - p_{MRC})^3] \tag{2.52}$$

BER for Alamouti (2x2) STBC case with BPSK modulation can be written as [49]

$BER_{Alamouti(2x2)}$

$$= p_{Alamouti}^4[1 + 4(1 - p_{Alamouti}) + 10(1 - p_{Alamouti})^2 + 20(1 - p_{Alamouti})^3]$$

$$(2.53)$$

2.6.5. Space-time trellis codes

The STTC is an extension of the conventional trellis code to the multi antenna systems [17]. The STTC provides a full diversity order like the STBC, but it also gives coding gain. The coding gain increases with the number of receiving antennas as well as the number of states. The STTC gives the coding gain by increasing the minimum distance between code sequences. Each STTC can be represented by a trellis diagram.

The encoder is implemented as s shift register. The STTC encoder with constraint length $v = 2$ and input block length $l = 2$ is shown in Figure 2.8.
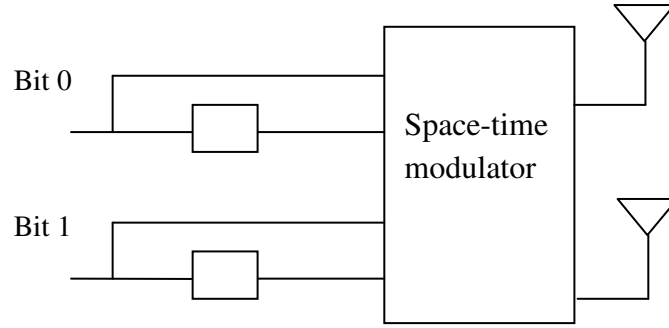
Fig. 2.8. The STTC Encoder

Each output symbol depends on the current input block, plus the two previous bits from the previous symbol period, stored in the two parallel shift registers. These are fed to a space-time modulator, which maps the four resulting bits to two modulated symbols to be transmitted through the two antennas.

The space-time modulator can be described by means of a generator matrix like that for conventional FEC codes. If the input data bits are in a vector form:

$$b = [\, b_i^0, b_i^1, \ldots, b_i^{l-1}, b_{i-1}^0, b_{i-1}^1, \ldots b_{i-1}^{l-1}, \ldots, b_{i-v+1}^0, b_{i-v+1}^1, \ldots, b_{i-v+1}^{l-1} \,] \qquad (2.54)$$

then the transmitted symbols are given by

$$s = Mod(bG)^T \qquad (2.55)$$

where G is the generator matrix and $Mod(.)$ denotes the modulation operation here.

A Simple STTC is shown in Figure 2.9 for a modulation consisting of two QPSK symbols. Two transmit antennas are used and the transmission achieves 2bits/s/Hz. The four possible symbols $\{1, j, -1, -j\}$ are labeled as $\{0,1,2,3\}$. The corresponding space-trellis has four incoming and outgoing branches per state. As common practice, the trellis is always initialized and ended at the zero state. A transition branch is chosen according to the state of the encoder and the input bits at time t. At time t, one symbol or two bits are transmitted at an antenna, depending on which transition state is made. The symbol transmitted at the other antenna is selected according to the previous state, and the two antennas choose their symbols for transmission based on the alternating state. A number of STTCs are described in the literature [17, 18]. Design criteria for codes are given in [19].
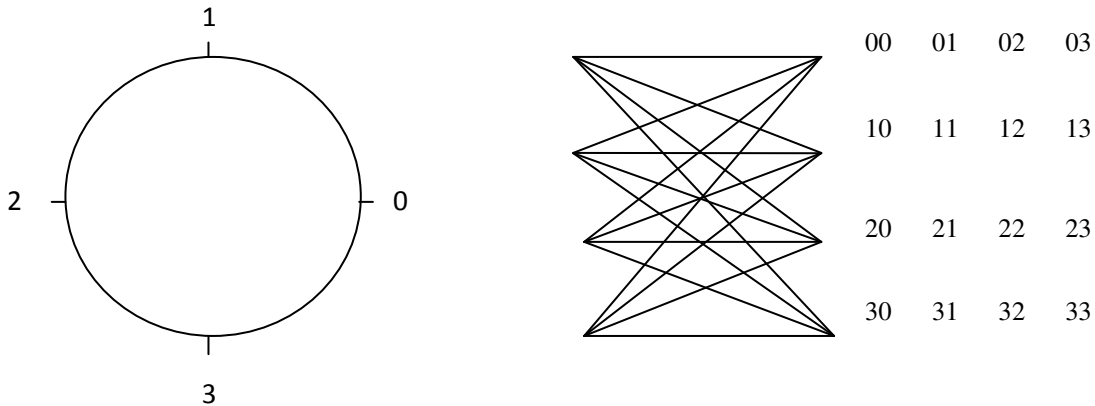
Fig. 2.9. Trellis of a four state QPSK STTC

2.6.6. Comparison of STBC and STTC

A comparison of STBC and STTC is given in Table 2.1, [12].

Table 2.1: Comparison of STBC and STTC

S.No	Space-time trellis coding	Space-time block coding
1	Has coding gain	No coding gain
2	Designing is very difficult	Designing is very simple based on orthogonal design
3	STTC outperforms with increasing trellis states and antennas	For 4-state code and one receive antenna, performance is similar to STTC
4	Decoding complexity very high	Easily decodable by ML decoding
5	Implementation complexity is high	Implementation complexity is less compared to STTC
6	Preserves capacity irrespective of the number of antennas.	Loses capacity with two or more receiving antennas

2.7. Orthogonal frequency division multiplexing

OFDM, also known as simultaneous MFSK, has been broadly implemented in high-speed digital communications in delay-dispersive environments. It is a multi-carrier modulation technique. In 1966, OFDM was first proposed by Chang. Chang introduced the principle of transmitting messages simultaneously over multiple carriers in a linear band-limited channel without inter symbol interference (ISI) and inter channel interference (ICI). The first version of OFDM employed a large number of coherent demodulators and oscillators. Discrete Fourier transform was applied to the modulation and demodulation by Weinstein and Ebert in 1971. To maintain frequency orthogonality over the dispersive channel, Peled and Ruiz proposed the notion of

cyclic prefix in 1980. The ETSI DAB standard is the first commercial OFDM-based wireless system proposed in 1995 [9].

2.7.1. Features of OFDM technology

In OFDM technology, the multiple carriers are called sub channels, and the frequency band occupied by the signal carried by a sub-channel is called sub-band. OFDM accomplishes orthogonality in both time and frequency domains [9].

The other advantages can be generally summarized as follows [9, 11]:

- OFDM can be efficiently implemented using FFT in the digital domain.
- OFDM is robust to multipath fading, due to the use of a cyclic prefix. So it can reliably transmit data over frequency-selective or time-dispersive channels without the need for a complex time domain channel equalizer.
- OFDM accomplishes robustness against narrow band interferences, since narrow band interference only affects a very small fraction of the sub-carriers.
- OFDM allows bandwidth-on-demand technology and higher spectral efficiency.
- OFDM is insusceptible to most forms of impulse noise thanks to the parallel transmission.
- Contiguous bandwidth for operation is not required.
- Frequency diversity can be exploited by coding and interleaving across sub-carriers in the frequency domain.

2.7.2. Principle of OFDM

For high-speed wireless communications, the multipath environment causes the channel to be frequency-selective. A frequency selective channel is equally divided into N frequency-flat

37

channels in OFDM system. Specifically, the N sub channels are assumed to be at frequencies

$$f_n = {}^{nW}\!/_N \, , n = 0,1, \dots \dots , N-1. \tag{2.56}$$

where W is the available total bandwidth, and usually $W = {}^N\!/_T$.

These sub-channels are orthogonal. Their inter carrier spacing is equal to ${}^1\!/_T$, the inverse of the symbol duration, and each sub-channel spectral peak must coincide with the zero-crossings of all the other sub channels. For PAM modulation with rectangular pulse shape, mutual orthogonality of the sub channels is seen from the relation

$$\int_{iT}^{(i+1)T} e^{j2\pi f_k t} \, e^{-j2\pi f_k t} dt = \delta_{nk} \tag{2.57}$$

OFDM leads to an equation of the same form as that of IFFT operation. Assuming that $d_{i,k}$ is the complex symbol to be transmitted on the ith sub channel at instant k, the transmitted signal is given by

$$s(t) = \sum_{k=-\infty}^{\infty} s_k(t) = \sum_{k=-\infty}^{\infty} \sum_{i=0}^{N-1} d_{i,k} \, g_i(t-kT) \tag{2.58}$$

where $g_i(t)$ is a normalized, frequency-shifted rectangular pulse

$$g_i(t) = \quad \frac{1}{\sqrt{T}} e^{j2\pi f_1 t} \, , 0 \le t \le T \tag{2.59}$$

$$0 \quad , \text{otherwise}$$

The complex symbol $d_{i,k}$ can be obtained by PSK, ASK, or QAM. Without loss of generality, for symbol $k = 0$, if the symbol is sampled at

$$t_u = {}^{uT}\!/_N \, , \, u = 0, 1, 2, \dots \dots , N-1. \tag{2.60}$$

we have

$$s_u = \frac{1}{\sqrt{T}} \sum_{i=0}^{N-1} d_{i,0} e^{j2\pi ui/N}$$

which is exactly the IFFT of the transmitted symbols. Thus, these modulations can be performed by using IFFT.

At the receiver, demodulation can be implemented by FFT. Due to the orthogonality property of the sub-channels, spectral overlapping among the sub-channels can be separated at the receiver. This makes the implementation much simpler than the traditional implementation that uses multiple oscillators.

2.7.3. OFDM transreceiver

OFDM is essentially a discrete implementation of multi-carrier modulation based on the principle of frequency division multiplexing (FDM). It utilizes digital modulation scheme via DFT. It divides the transmitted bit stream into many different parallel sub-streams, typically dozens to thousands. By doing so, the wide-band frequency selective channel is divided into a number of parallel narrow-band sub-channels, and each of the low rate data streams is transmitted over one sub-channel. Typically, the sub-channels are orthogonal and number of sub channels is chosen such that each sub-channel has a bandwidth that is much less than the coherence bandwidth of the channel. Thus, inter symbol interference on each sub-channel is very small. Based on this reason, OFDM is extensively used in many high data rate wireless communication systems. A schematic block diagram of an OFDM system is shown in Figure 2.10.

39
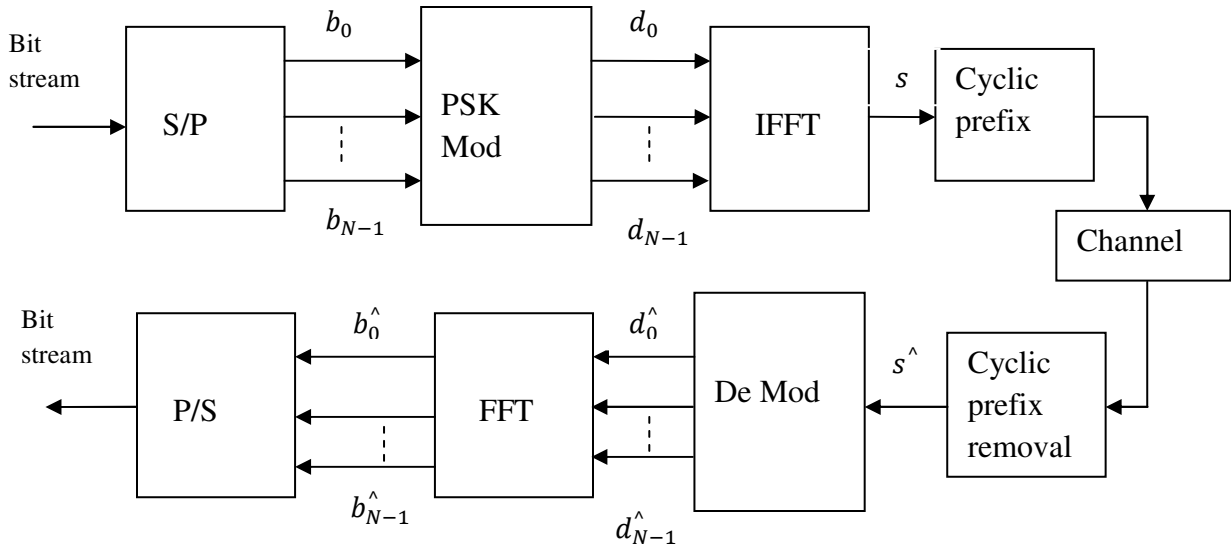
Fig. 2.10. Block diagram of OFDM

First, the serial to parallel converter converts the bit stream into a number of parallel bit streams. Then, the bit streams are modulated according to an M-ary modulation. Then, each block of bits is forwarded to the IFFT and transformed into an OFDM signal. After that, the cyclic prefix will be appended to the OFDM signal by copying the last N_{CP} samples to the top of the current OFDM block. For the purpose of ISI elimination, the length of the cyclic prefix is chosen to be larger than the maximum path delay of the channel. Then, the OFDM blocks are converted to serial signals and sent out. At the receiver, assuming a perfect timing and carrier frequency synchronization, first the received signals are converted to parallel signals and then the cyclic prefix removed. After going through the FFT block, with the estimated channel information the data symbols are detected. Thus, OFDM modulation with cyclic prefix transforms a frequency selective channel into N perfectly flat fading sub channels on which SFBC transmitter diversity can be applied.

2.8. MIMO-OFDM system

In broadband wireless systems, the MIMO channels are affected by the frequency-selective fading. This fading effect complicates the design of ST codes because of ISI. To solve this problem, OFDM can be combined with MIMO systems, and this is referred to as MIMO-OFDM. The combination of MIMO and OFDM has the potential of meeting this stringent requirement since MIMO can improve the capacity and the diversity, and OFDM can mitigate the effects due to multipath fading. The schematic block diagram of the MIMO-OFDM system is shown in Figure 2.11.
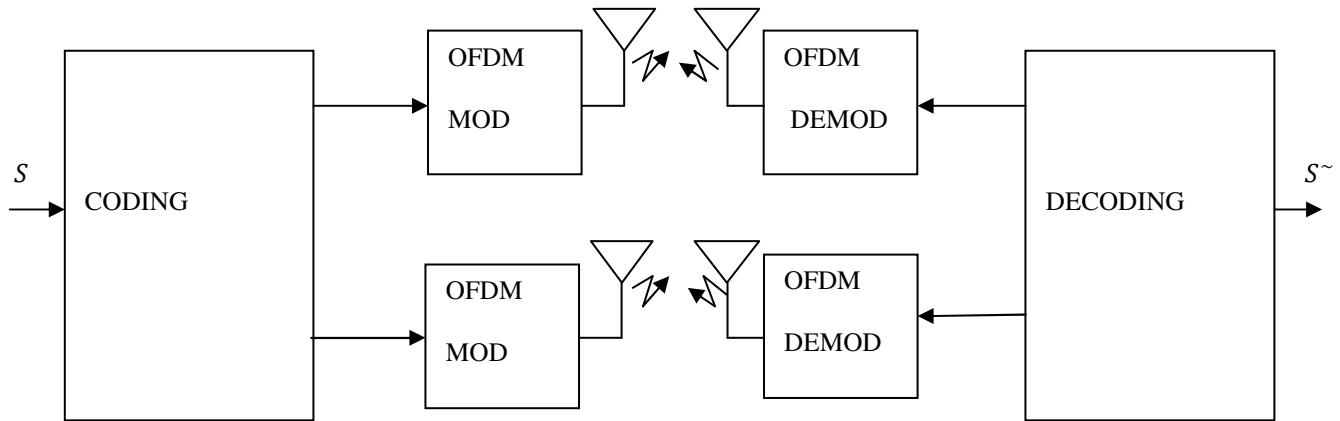
Fig. 2.11. Block diagram of MIMO- OFDM

The schematic block diagram of MIMO-OFDM system with M_t transmit, M_r receive antennas and N-tone OFDM is illustrated in this figure. The incoming bit stream is first mapped into a number of data symbols via some modulation type such as BPSK, QPSK, and QAM. Then, blocks of data symbols are encoded and transmitted through M_t transmit antennas in T OFDM

blocks. Each block has N sub channels. After appending the cyclic prefix on each OFDM block, the blocks are transmitted through M_t transmit antennas.

After passing through the MIMO channels, first the received signals are sent to the reverse OFDM (cyclic prefix removal, DFT) and then sent to the decoder. If the channel state information (CSI) is available at the receiving side, the optimal ML detection is performed.

2.8.1. Space-time coded OFDM

The ST coding for a MIMO-OFDM with two transmit antennas is depicted in Figure 2.12
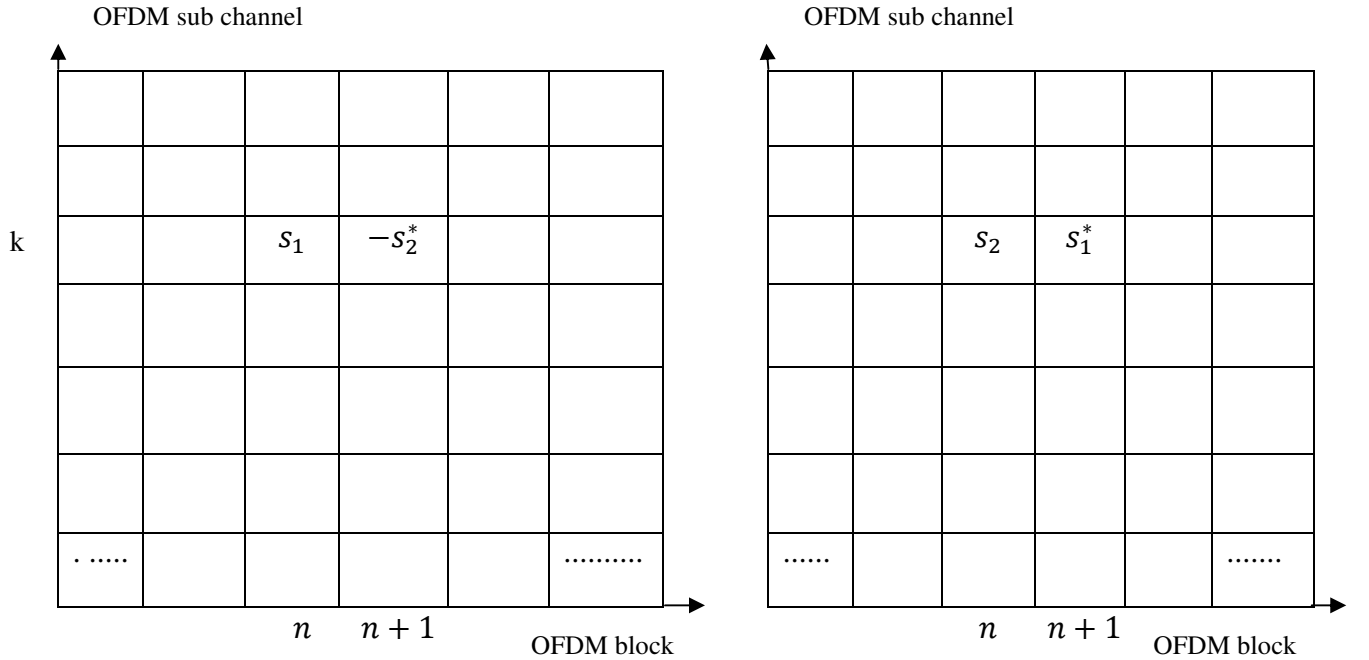
Fig. 2.12. Space-time Coding

Two information symbols s_1 and $-s_2^*$ are transmitted through the sub-channel k of antenna 1 in OFDM blocks n and $n+1$, respectively. Meanwhile, s_2 and s_1^* are transmitted through sub channel k of antenna 2 in OFDM blocks n and $n+1$, respectively. Although The ST coded

OFDM exploits the space diversity, the multipath diversity which is offered by frequency-selective fading channels, is not exploited.

2.8.2. Space-frequency coded OFDM

This startegy, which consists of coding across antennas and OFDM sub channels, is called SF coding [20]. In SF coding, the almouti code directly spreads over two sub channels in one OFDM block.

The SF coding for a MIMO-OFDM with two transmits antennas is depicted in Figure 2.13.
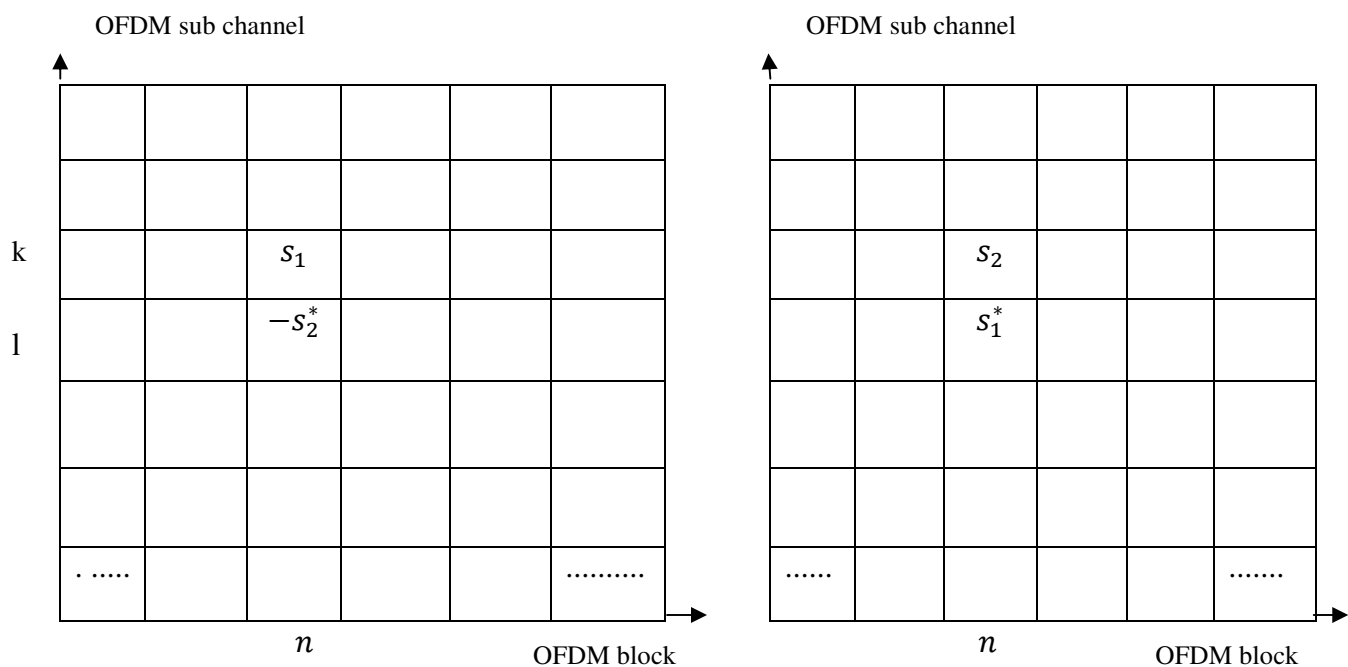
Fig. 2.13. Space-frequency Coding

Two information symbols s_1 and $-s_2^*$ are transmitted through two different sub-channels $k \; and \; l$ of antenna 1 in OFDM block n, respectively. Meanwhile, s_2 and s_1^* are transmitted through sub channels k and l of antenna 2 in OFDM block n, respectively.

2.9. Conclusion

In this chapter, we have provided the necessary background material for the implementation of different transmission schemes over fading channels. First, basic concepts of wireless communications such as wireless channel, and fading have been presented. Then, existing MIMO techniques have been described. In particular, MIMO systems, MIMO channel, capacity of the MIMO channel, and space time coding have been presented. Finally, OFDM technique and MIMO-OFDM systems have been discussed.

CHAPTER 3

DIGITAL WATERMARKING

In this chapter, we briefly discuss the basic digital watermarking techniques, medical image watermarking, and propose a new medical image watermarking scheme.

3.1. Introduction

Digital watermarking is a technique to embed copyright information or other information into an image or video or audio. It is one of the best solutions to prevent illegal modifying, copying, and redistributing multimedia information.

Digital watermarking algorithms should maintain few basic requirements [21]:

- **Imperceptibility:** The watermark should not degrade the perceptual quality of the host signal; thus, the difference between the watermarked and original documents should be unnoticeable to an observer.

- **Capacity:** The number of information bits that can be embedded into the original media in one second.

- **Robustness:** It should not be possible for the watermark data to be removed by unauthorized distributors; thus, it should be robust to resist common signal processing operations such as compression and filtering.

- **Security:** The watermark should be extractable by only authorized persons.

- It should be possible to extract the watermark without knowledge of the original signals.

- The watermark should not be extractable without prior knowledge of the embedded watermark.

- The watermark is embedded directly in the signals, not in a header of the signal.

3.1.1. Types of watermarking systems

Watermarking methods can be classified into different categories depending on various criteria. According to the type of documents to be watermarked, the watermarking systems can be classified in to four categories: text watermarking, audio watermarking, image watermarking and video watermarking. A watermarking system can be classified according to whether or not the original media and the secret key information are needed in the watermark extraction algorithm as blind, semi-blind, and non-blind watermarking systems. According to their robustness against attacks, watermarking techniques can be classified as robust, fragile, and semi fragile. According to the perceptibility of the watermark, watermarking schemes can be classified as visible, invisible and dual watermarks.

Blind watermarking system: This is also referred to as public watermarking. This type of watermarking technique requires only the secret key during the extraction of the watermark.

Semi-blind watermarking system: This is also called semi-private watermarking. This type of watermarking system requires the secret keys and copy of the embedded watermark information.

Non-blind watermarking system: This is also called private watermarking. This type of watermarking system requires the original image, the secret key, and the watermark information for watermark extraction.

Visible watermark: The watermark information is embedded into an image in such a way that the watermark is intentionally visible to the observer. The major purpose of this technique is to prevent unauthorized commercial use of the information.

Invisible watermark: The watermark information is embedded into the host image such that the watermark is not visible to the viewer, but may be detected by a computer program. This watermark is used as an evidence of ownership.

Dual watermark: This is a combination of invisible and visible watermarks. An invisible watermark is utilized as a backup for the visible watermark.

3.1.2. Classification of watermarking methods

According to the domain for watermark embedding, digital watermarking methods can be classified into two basic categories: spatial domain methods and transform domain methods.

Spatial domain methods: In these methods, the lower order bits of the image pixels are replaced with that of the watermark. Spatial domain methods are not robust against attacks, but their computational complexity is less [22].

Transform domain methods: Here, the original image is transformed into the frequency domain by using a transform such as Fourier transform, discrete cosine transforms (DCT) or discrete wavelet transform (DWT). Then, watermarks are added to the values of its transform coefficients. After performing the inverse transform, the watermarked image is obtained [22]. Differences between the spatial domain and transform domain methods are summarized in Table 3.1.

Table 3.1: Differences between spatial domain and transform domain methods for watermarking		
	Spatial domain	**Transform domain**
Perceptual quality	High	Low
Robustness	Fragile	More robust
Capacity	High (depends on the size of an Image)	Low
Computational Cost	Low	High

3.1.3. General frame work for digital watermarking

The general frame work for digital watermarking is as shown in Figure 3.1. The watermark embedding system has the original image, the secret key, and the watermark as inputs, and watermarked image as the output. The extraction process has the watermarked image, the secret key, the original image or the original watermark or both as inputs. The output of the extraction algorithm is either suspect watermark or some confidence measure [21].
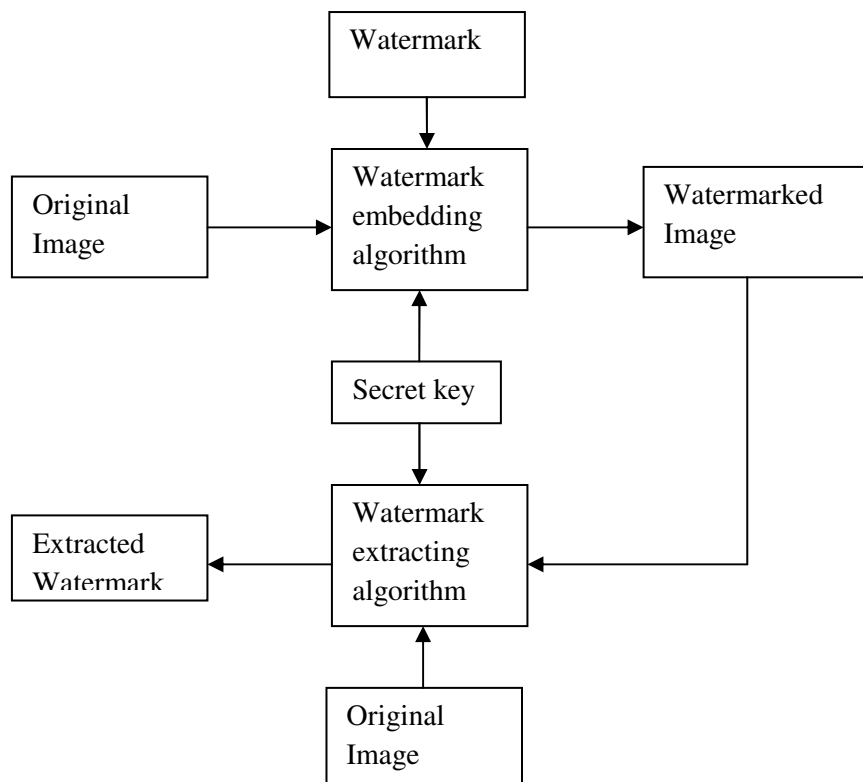
Fig. 3.1. Watermark embedding and extracting model

3.2. Medical image watermarking

These days, telemedicine is increasingly being used in conventional medicine, to permit doctors the world over to share exclusive recourses and valuable experience. Hence, healthcare industry demands robust, secure, and reliable information hiding techniques promising strict secure communication and authentication through wireless networks. So the security aspect of the data hiding is also an important parameter as far as the medical field is concerned.

Digital watermarking in medical images is very important to prevent modification of the medical images by the other parties. Embedding patient information into the medical images is also helpful to reduce the storage requirements, but medical image watermarking requires extreme care when embedding data into the medical images.

3.2.1. Requirements for medical image watermarking

In the medical field, the qualities of the medical images are very important in order to be able to diagnose accurately and hence, the images shall not be modified in any way. In order not to affect the medical image quality, there are several constraints and important requirements that should be looked into medical image watermarking. As stated in [23], three important requirements in the medical image watermarking are imperceptibility, integrity control, and hiding capacity. In medical image watermarking, an embedded watermark should not be visible under normal observation, and it must not affect the quality of the image, as well. The watermarked image must be perceptually imperceptible. Integrity control of the watermarked image is an important requirement in the medical image watermarking in the context of legal aspects. Thus, there is a need to prove that the images, on which the diagnoses and any insurance claims are based on, have preserved their integrity [23]. Watermarking as a tool for integrity

control is adapted for the purposes of electronic patient records (EPR) which are used to keep the information of the patient and distribution of the same that take place in hospital [24, 25]. Hiding capacity is the size of the information that can be hidden to the relative size of the original image. It is very important that the diagnosis data and personal information can be embedded into an original image [26]. Bits of the hiding capacity depend on the total information, to be embedded, as long as the watermarked image is imperceptible under visual perception.

3.2.2. Medical image watermarking domain

In medical image watermarking, the patient information (watermark) is either embedded in the spatial domain or transform domain. In the spatial domain method, watermark bits are embed into the LSB of grayscale values of the pixels in the original image. This method does not damage the important information in the original images if the watermark is embedded in the background of the images, but this domain is very vulnerable to attacks. In the transform domain method, the image is transformed into the frequency domain (using DFT or DCT or DWT) and the watermark is added to the corresponding coefficients. This method is more robust than the spatial domain method against attacks, but some of the information in the original images undergoes mild modifications. So image quality is degraded in the transform domain method. In the medical imaging applications, there are stringent constraints on image fidelity that strictly prohibit any permanent image degradation by the digital watermarking. For instance, quality degradation in the medical image due to digital image watermarking may cause an incorrect diagnosis, which may lead to possible life-threatening consequences. Because of the image degradation, transform domain is not preferred in medical image watermarking.

3.2.3. Proposed medical image watermarking scheme

A medical image watermarked scheme introduced in [27] has utilized an advanced encryption standard (AES) algorithm for encryption, and an RS error correction code to enhance the robustness. To enhance the robustness of the embedded watermark, we propose an RS-LDPC concatenated error correction code.

A block diagram of the proposed scheme is shown in Figure 3.2. At the watermark embedding side, the text data of the patient information is first encrypted using the encryption algorithm to prevent unauthorized access of the data. The watermark consists of sequence of ASCII codes, which is encrypted by taking the logarithm of the ASCII codes. The encryption algorithm can be mathematically stated as [3]

$$p_e = log\ (p_0 * 2 + 100) - 300 \qquad\qquad (3.1)$$

where p_e is the encrypted watermark and p_0 is the ASCII code of the original watermark. The encrypted watermark (p_e) is stored as an integer. Then, the encrypted information is coded by concatenation of Reed Solomon (RS) codes [10] and low density parity check codes (LDPC) [28, 29] for robustness. The RS-LDPC coded encrypted watermark bit streams are swapped with the least significant bit (LSB) of the image. Each bit of the code thus replaces lowest significant bit (LSB) of one pixel in the image. This process of coded bits embedding in consecutive image pixels is repeated to include all the bit streams. The LSB of the pixel is chosen so as to ensure the degradation of the image is minimal. The embedding process causes redistribution among all the even and odd pixels. If a bit 0 of the watermark replaces the LSB of a pixel with even grey value in the image, the LSB of the watermarked image pixel also remains to be 0; if bit 1 replaces the LSB, the LSB of the watermarked image pixel becomes 1. Thus, under no noise conditions, the

bit 0 or 1 of the watermark can be extracted exactly from the image. However, if a 0 or 1 of the watermark replaces the LSB of a pixel with odd grey value of the image, then the bit 0 is extracted as 1 and 1 extracted as 0. Thus, the accuracy of the extracted watermark depends on the region of the image into which it is embedded. Hence, LSBs of a pixel with odd grey value of the image are set to zero in a region of the image into which the watermark is to be embedded. At the watermark extraction side, the encrypted and RS-LDPC coded watermark extraction unit, an RS-LDPC concatenated decoder, and a decryption unit perform, in the reverse order to that at the watermark embedding side. It may be mentioned that the decrypted watermark is obtained by

$$p_0 = exp\{(p_e + 300)/100\} - \log{(2)}\} \qquad (3.2)$$

Equation (3.2) yields the exact reconstruction, even when p_e is rounded off to the nearest integer.
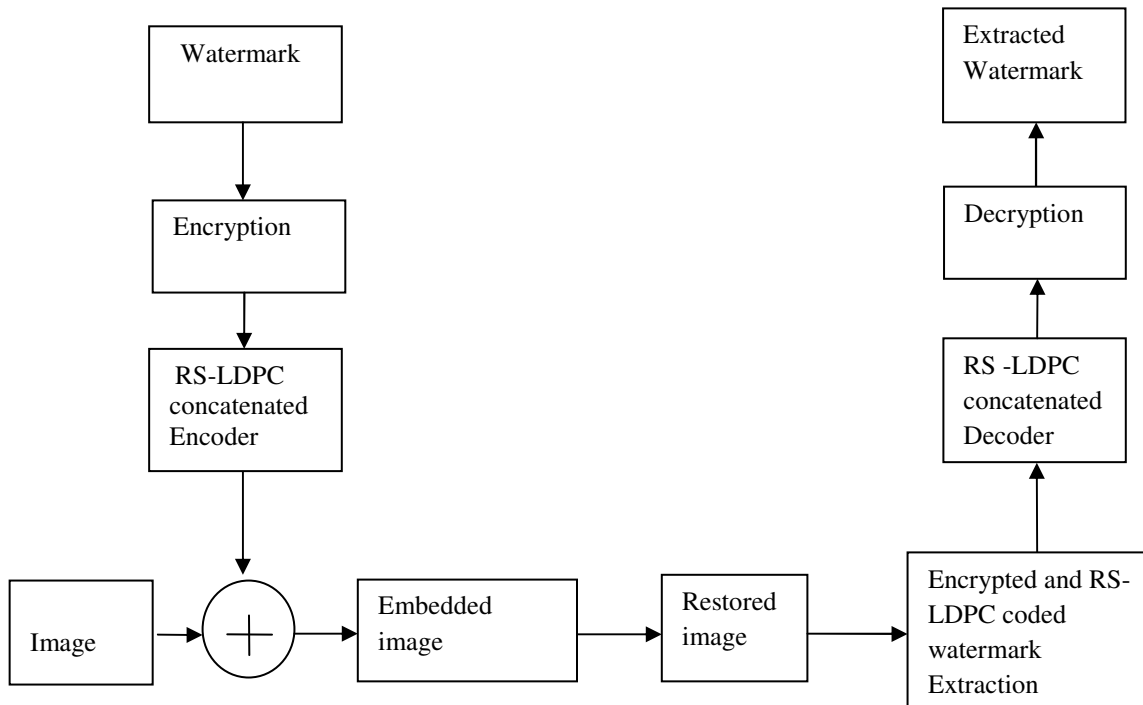
Fig. 3.2. Block diagram of robust digital watermarking scheme

3.3. Conclusion

In this chapter, first we briefly studied about the digital watermarking techniques, medical image watermarking concepts, and later proposed a new medical image watermarking scheme. This scheme is utilized for digital watermarking in the proposed transmission schemes of this thesis.

CHAPTER 4

WATERMARKED MEDICAL IMAGE TRANSMISSION OVER IMPULSIVE NOISY WIRELESS CHANNELS

In the previous chapters, we briefly described the digital watermarking techniques and wireless communication concepts. These are useful concepts for the remaining part of the thesis. In this Chapter, we propose a robust scheme for watermarked medical image transmission over impulsive noisy wireless channels. The effectiveness of the proposed approach is demonstrated through the simulation results on a watermarked medical image.

4.1. Introduction

Now a days, exchange of medical images between hospitals located in different geographical locations is a common practice. This databases exchange requires efficient and reliable transmission and storage techniques to reduce the health care cost. This exchange involves a large amount of vital patient information, such as medical images and text data. It needs excessive memory and causes transmission overheads when handled separately using information media like the internet. By embedding the text files as watermark into the medical images, the data security and efficient memory utilization can be achieved. To enhance the security, the watermark is to be encrypted before embedding it into the medical image of the patient. The medical image watermarking process has been discussed in the Chapter 3. Further, it is very important to preserve all the describing features of the image during medical image

transmission, so that the diagnosis is error free. For this reason, the lossy techniques, which tend to produce high compression ratios, are not permissible in the medical image compression [2]. JPEG with DCT compression is optimized for visual perception. Hence, in order not to lose the important information contained in the medical images, lossless JPEG (compression ratio. 1.6:1) is preferred [3]. However, even this low ratio compression may not be acceptable on watermarked medical images to protect all the features of the image. Hence, it is necessary to transmit watermarked medical images without compression.

Further, the wireless channels have fluctuating channel characteristics and high bit-error rates. These impairments make the reliable transmission of the compressed image very difficult in a wireless channel. During the image transmission over wireless channels, the lost or errant data is to be recovered from the received data. A remedy for this problem is the Shannon's well-known joint source-channel coding [30]. The turbo channel coding provides the near–Shannon capacity error correcting performance, when iterative soft decoding is employed [31]. Hence, in this chapter, a robust scheme is proposed for transmission of watermarked medical images over impulsive noisy wireless channels. This scheme starts by robust watermark embedding process. Then the watermarked medical image is turbo coded for its robust transmission over impulsive noisy wireless channels. The noisy scenario is simulated by generating impulsive noise using the model given in [32]. By adding impulse noise to the embedded image, the robustness of the proposed approach is demonstrated for restoration of the image and extraction of watermark [33]

4.2. Proposed scheme for transmission over an impulsive noisy channel

The schematic block diagram of the proposed scheme is depicted in Figure 4.1. At the transmitter side, it consists of the robust watermark embedding unit, which has already been

discussed in chapter 3, a JPEG encoder to encode the watermarked image, and a turbo encoder to add redundancy to the coded watermarked image. At the receiver side, an error protection turbo decoder, a JPEG decoder, and watermark extracting unit perform, in the reverse order to that at the transmitter. JPEG encoding and decoding process is shown in Figure 4.2. The complete turbo encoding and decoding process is as given in [6].
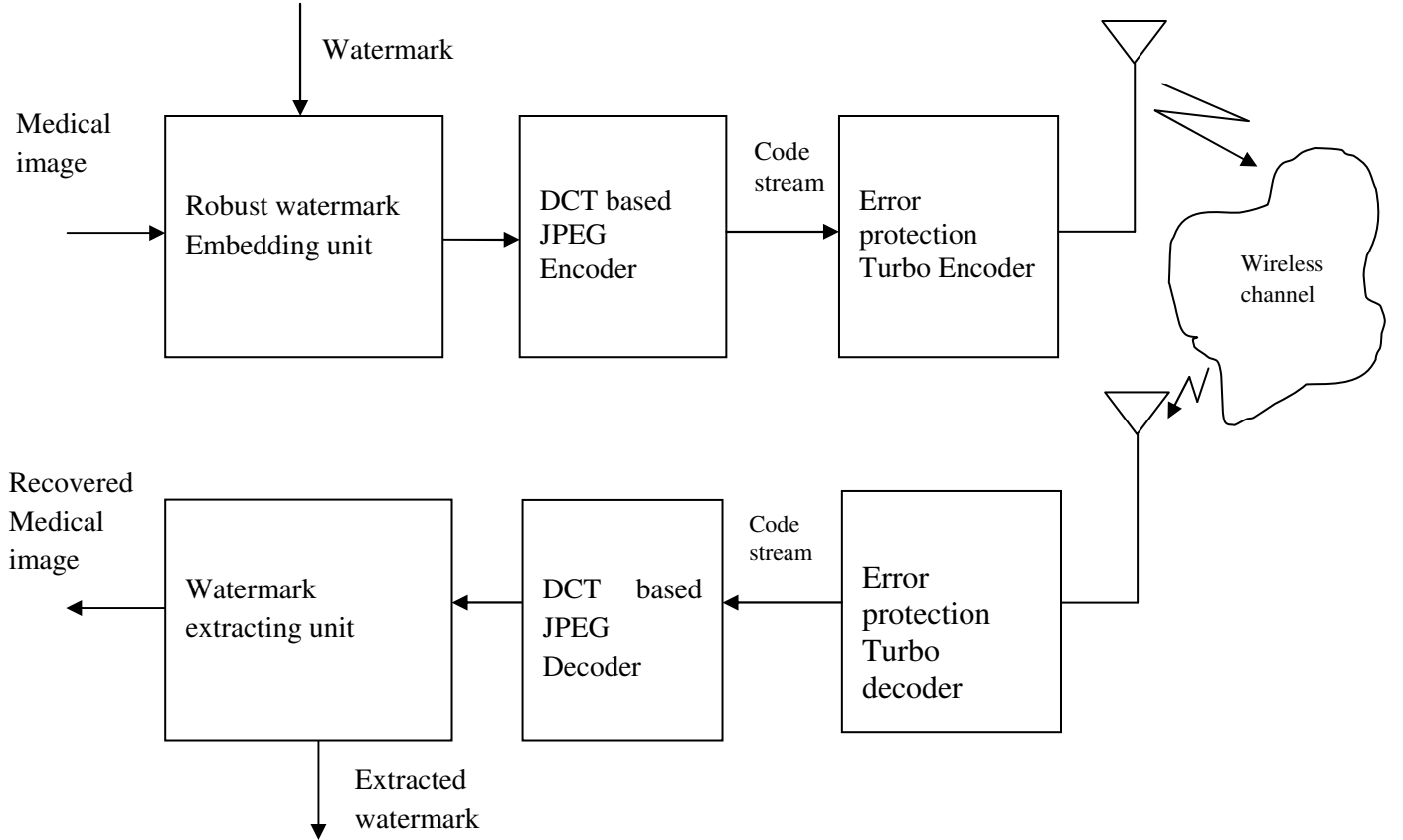
Fig. 4.1. The schematic block diagram of the transmission system

The Impulsive noise model

The widely used two-term Gaussian mixture model is used for the impulsive noise. The probability density function (PDF) of this noise model has the form [32]

$$\eta = (1-\varepsilon)\aleph(0,\nu^2) + \varepsilon\aleph(0,\kappa\nu^2) \,, \tag{4.1}$$

with $v > 0, 0 \leq \varepsilon \leq 1$ and ≥ 1 . Here, the $\aleph(0, v^2)$ term represents the background noise, and the $\aleph(0, \kappa v^2)$ term represents an impulsive component, with ε representing the probability that impulses occur. The noise variance is given by $\sigma^2 = (1 - \varepsilon)v^2 + \varepsilon k v$.

JPEG encoding and decoding

The schematic block diagrams of the encoder and decoder used in the JPEG standard are illustrated in Figure 4.2.

Input image → Block extractor → DCT → Quantizer → Symbol Encoder → Compressed image

(a)

Compressed image → Symbol Decoder → De - quantizer → Inverse DCT → Block merger → Reconstructed image

(b)

Fig. 4.2. The schematic block diagram of JPEG a) Encoder b) decoder

As can be seen from the block diagram, the DCT- based JPEG compression is performed in four sequential steps: sub-image extraction, DCT computation, quantization, and variable-length code assignment. The complete description of the JPEG is given in [34].

4.3. Implementation of the proposed scheme

The scheme proposed in the previous section is implemented using MATLAB to illustrate its performance on a watermarked medical image. A typical patient information (text file) shown in Figure 4.3 (a) is considered as the watermark and encrypted using the algorithm explained in Section 3.2.3. The 8 bit ASCII codes of the encrypted text are shown in Figure 4.3 (b). The encrypted watermark is broken into bit streams and coded with (31,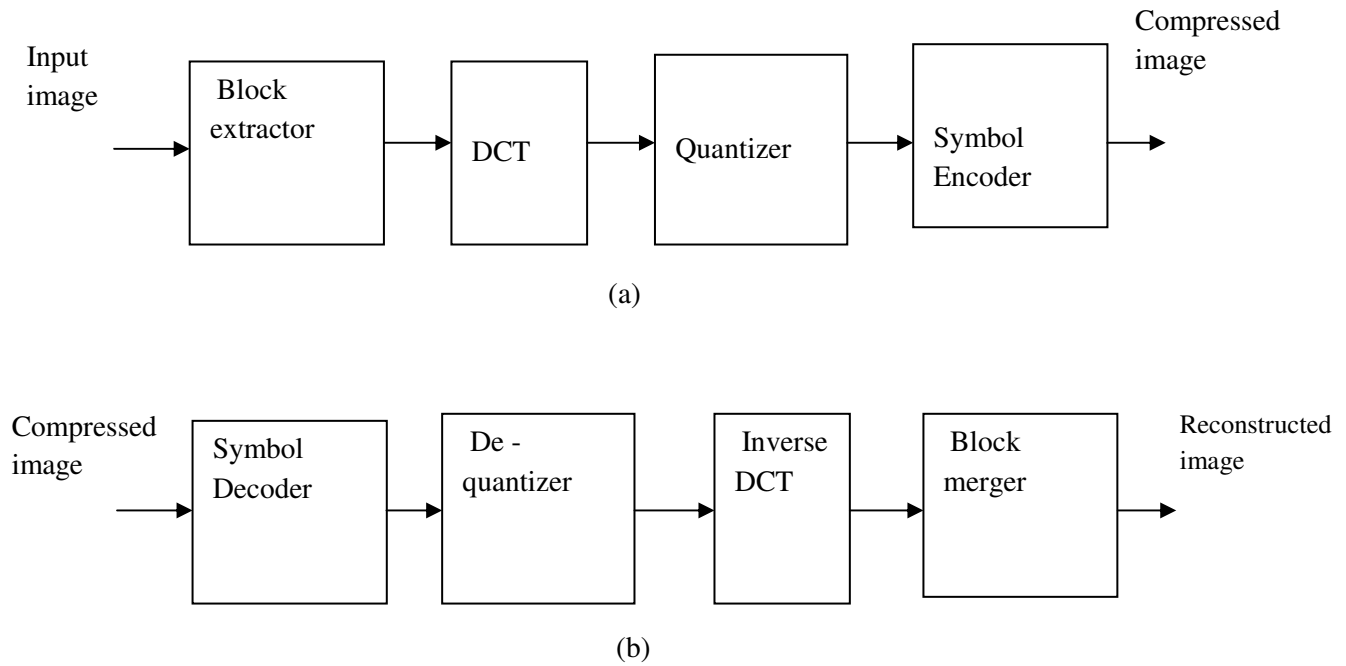 15) RS encoder with code word length of 31 and RS coded encrypted message word length of 15 with an error correcting capability of 8. The watermark is further coded using an LDPC encoder of rate ½. The RS-LDPC code words are broken into bits and embedded as watermark into the pixels of a region of a magnetic-resonance- imaging (MRI) image as explained in the embedding process. The MRI image of size $500 \times 383 \times 3$ with brain tumor (which appears as a white area at lower left side of the image) with embedded watermark is shown in Figure 4.4. As can be seen from Figure 4.4, the embedding process does not affect the image quality. This is attributed to the fact that the change in the LSB of a pixel changes its brightness by one part in 256. The noisy scenario is simulated by generating impulsive noise using an equation (4.1) with $\varepsilon = 0.01$ and $k = 100$ so that signal-to-noise ratio (SNR) is 4dB. The punctured turbo codes with rate $^1/_2$ and turbo decoding with two iterations are used. The BPSK modulation technique is used in this approach. The watermark is extracted from LSBs of the restored image and decoded using RS-LDPC concatenated decoding and decrypted using the decryption algorithm described in Section 3.2.3. The restored MRI image and the extracted watermark at $SNR = 4dB$ without turbo coding are shown in Figures 4.5 and 4.6, respectively whereas the restored image and the extracted watermark with turbo coding (with two iterations decoding) at $SNR = 4dB$ are shown in Figures 4.7 and 4.8, respectively. From Figures 4.7 and 4.8, it is observed that the restored

image resembles the original MRI brain image and the extracted watermark is same as the original watermark shown in Figure 4.3 (a). From the results, it is clear that the proposed approach is effective for watermarked medical image transmission over impulsive noisy wireless channels.

> **CARE**
>
> **HYDERABAD**
>
> **PATIENT NAME: JOSEPH**
>
> **AGE: 45**
>
> **BP: NO**
>
> **BS: NO**

(a)

> **¾ » Ò Á**
>
> **Å Ú ¿ Á Ò » ¼ » ¿**
>
> **Ð » Ô Æ Á Í Ô t Í » Ì Á ⁻ È Î Ó ÁÐ »**
>
>   **» Ä Á ⁻ ¤ ¦**
>
> **¼ Ð⁻ Í Î**
>
> **¼ Ó⁻ Í Î**

(b)

Fig. 4.3 (a) Watermark (b) encrypted watermark

Watermark embedded Region
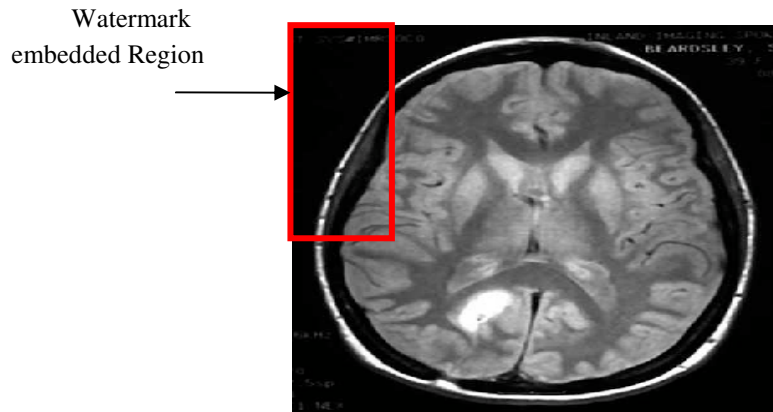
Fig. 4.4. MRI brain image with embedded watermark
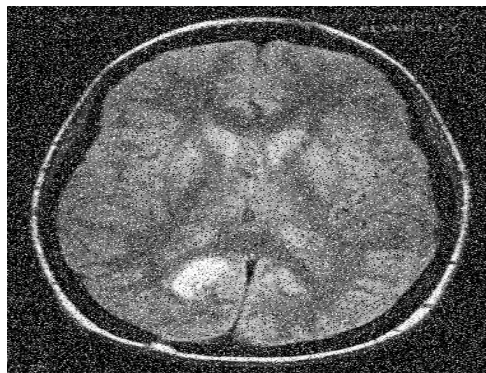
Fig. 4.5. Recovered MRI brain image without turbo coding at $SNR = 4dB$ with RS-LDPC coded embedded watermark.

DDYE

EZDHR@D&D

W8TIHNT S"ME:NAKLS\PG

/GQ845

BP: NO

BS: NO

Fig. 4.6. Extracted watermark without turbo coding at $SNR = 4dB$
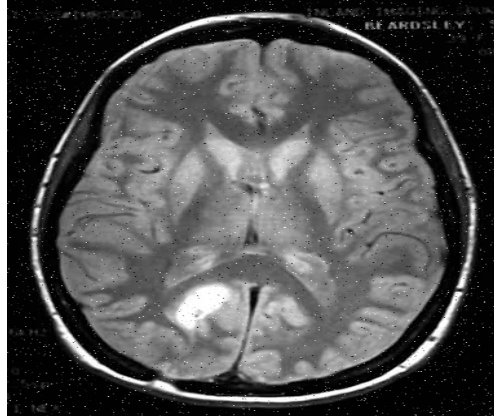
Fig. 4.7. Recovered MRI brain image with turbo coding   at $SNR = 4dB$ with RS-
LDPC coded embedded watermark

CARE

HYDERABAD

PATIENT NAME: JOSEPH

AGE: 45

BP: NO

BS: NO

Fig. 4.8. Extracted watermark with turbo coding at $SNR = 4dB$

4.4. Conclusion

In this Chapter, we have proposed a robust approach for the transmission of medical images over wireless channels with concealed patient information as watermark. The proposed approach has been demonstrated by transmitting a watermarked MRI image over an impulsive noisy channel. From the results, it is clear that the restored image and the watermark are exactly extracted at $SNR = 4dB$ using the proposed approach that includes turbo coding.

CHAPTER 5

MIMO SCHEME FOR WATERMARKED MEDICAL IMAGE TRANSMISSION OVER RAYLEIGH FADING CHANNELS

In chapter 4, we proposed a scheme for transmission of watermarked medical images over an SISO channel. However, an SISO Channel has some disadvantages including limited channel capacity. To overcome these disadvantages, we propose, in this chapter, a new MIMO scheme for transmission of watermarked medical images over Rayleigh fading channels in this Chapter. The efficacy of the proposed scheme is demonstrated through experimental results.

5.1. Introduction

Wireless systems are developing rapidly to provide voice, data and multimedia messaging services. These services require reliable wireless channels with large capacities. Systems which communicate over an SISO wireless channel have limited capacity. Also, in some situations, communication over a SISO channel is not reliable due to multipath fading, which is inevitable in scattering environments that are subject to changes over time. The spatial diversity from multiple antennas at the transmitter (Tx) and the receiver (Rx) enables MIMO techniques to be effective against channel fading [35-37] and the technology has been standardized [38-39]. The most commonly used channel model for MIMO systems is independent flat Rayleigh fading.

In MIMO multiplexing transmission, the channel capacity can be linearly increased in proportion to the number of antennas and a large capacity transmission can be achieved [40]. As such, in

this chapter, we propose a scheme with a MIMO channel for transmission of watermarked images. This scheme starts by a robust digital watermark embedding process and then the watermarked medical image is transmitted through a BPSK modulator, a serial to parallel conversion unit, and multiple antennas.

The structure of this chapter is as follows. In Section 5.2, we briefly discuss about the background concepts such as maximum likelihood detection for MIMO. In Section 5.3, we propose a new MIMO scheme for transmission of medical images over Rayleigh fading channels. Section 5.4 deals with the implementation of the proposed scheme. Section 5.5 consists of a number of experiments validating the efficacy of the proposed scheme. Finally, Section 5.6 summarizes the major contributions of this chapter.

5.2. Maximum likelihood detection for MIMO

Wireless MIMO systems promise improved performance compared to conventional systems. Techniques for achieving these advantages [41]-[43] include zero forcing (ZF) detection, maximum likelihood (ML) detection, minimum mean square error (MMSE) detection, and vertical-Bell laboratories layered space-time (V-BLAST) mechanism. Among all these techniques, ML detection is optimum in terms of minimizing the overall probability and, with small number of antennas and low-order constellations; also, the complexity of ML detection is not overwhelming [44]. ML detection is a preferred method of parameter estimation in statistics. It is an important tool for many statistical non-linear modeling techniques.

ML detection finds the vector symbol $J \in \mathbb{Q}^{M_T}$ that has most likely been transmitted. Under the usual assumption of i.i.d. proper complex Gaussian noise and assuming that all possible

transmitted vector symbols $x^{\wedge} \in \mathbb{Q}^{M_T}$ are equally likely to occur; the corresponding detector can

be expressed as [45]

$$J = \arg\min_{J \in \mathbb{Q}^{M_t}} \|y - Hx^{\wedge}\|^2$$

$$= |y - Hx^{\wedge}|^2 \tag{5.1}$$

where H is the channel coefficients matrix, y is the received vector and M_t is the number of

transmitting antennas. A straightforward implementation solves (5.1) by exhaustively searching

over the entire set of possible vector symbols($\mathbb{Q}^{M_T}$) to find J.

(i) Maximum likelihood detection for 2X2 MIMO

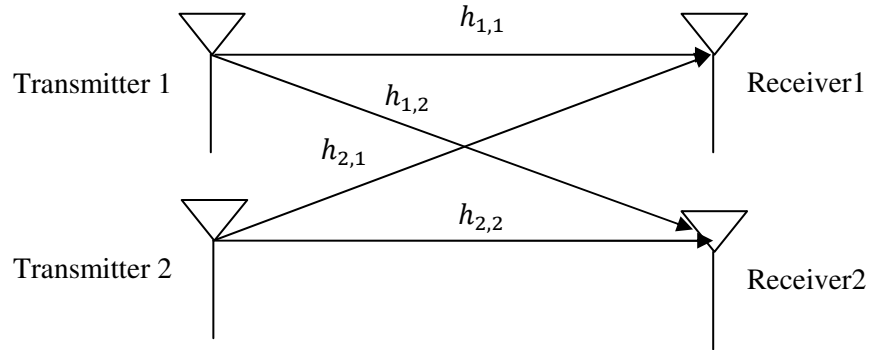For simplicity, let us consider a 2x2 MIMO channel, as shown in Figure 5.1.

Fig. 5.1. 2X2 MIMO Channel model

The received signal for the 2×2 MIMO channel can be expressed as

$$y_j = \sum_{i=1}^{2} h_{j.i} x_i + n_j, \quad j = 1, 2 \tag{5.2}$$

where x_i ($i = 1, 2$) are the transmitted symbols, n_j ($j = 1, 2$) are noise samples, and $h_{j,i}$ are the impulse responses of the channels from the i th transmit antenna to j th receive antenna. The above equation can be represented in matrix form as

$$\begin{bmatrix} y_1 \\ y_2 \end{bmatrix} = \begin{bmatrix} h_{1,1} & h_{1,2} \\ h_{2,1} & h_{2,2} \end{bmatrix} \begin{bmatrix} x_1 \\ x_2 \end{bmatrix} + \begin{bmatrix} n_1 \\ n_2 \end{bmatrix} \tag{5.3}$$

In the case of 2×2 MIMO, ML detection minimizes

$$J = \left| \begin{bmatrix} y_1 \\ y_2 \end{bmatrix} - \begin{bmatrix} h_{1,1} & h_{1,2} \\ h_{2,1} & h_{2,2} \end{bmatrix} \begin{bmatrix} \hat{x}_1 \\ \hat{x}_2 \end{bmatrix} \right|^2 \tag{5.4}$$

If the modulation is BPSK, the possible values of x_1 are $+1$ or -1, similarly x_2 also takes values $+1$ or -1. So, to find the ML estimate, we need to find the minimum from the all four combinations of x_1 and x_2 with J defined for the four combinations as

$$J_{+1,+1} = \left| \begin{bmatrix} y_1 \\ y_2 \end{bmatrix} - \begin{bmatrix} h_{1,1} & h_{1,2} \\ h_{2,1} & h_{2,2} \end{bmatrix} \begin{bmatrix} +1 \\ +1 \end{bmatrix} \right|^2 \tag{5.5}$$

$$J_{+1,-1} = \left| \begin{bmatrix} y_1 \\ y_2 \end{bmatrix} - \begin{bmatrix} h_{1,1} & h_{1,2} \\ h_{2,1} & h_{2,2} \end{bmatrix} \begin{bmatrix} +1 \\ -1 \end{bmatrix} \right|^2 \tag{5.6}$$

$$J_{-1,+1} = \left| \begin{bmatrix} y_1 \\ y_2 \end{bmatrix} - \begin{bmatrix} h_{1,1} & h_{1,2} \\ h_{2,1} & h_{2,2} \end{bmatrix} \begin{bmatrix} -1 \\ +1 \end{bmatrix} \right|^2 \tag{5.7}$$

$$J_{-1,-1} = \left| \begin{bmatrix} y_1 \\ y_2 \end{bmatrix} - \begin{bmatrix} h_{1,1} & h_{1,2} \\ h_{2,1} & h_{2,2} \end{bmatrix} \begin{bmatrix} -1 \\ -1 \end{bmatrix} \right|^2 \tag{5.8}$$

(ii) Maximum likelihood detection for 4X4 MIMO

Let us consider a 4x4 MIMO channel, as shown in Figure 5.2
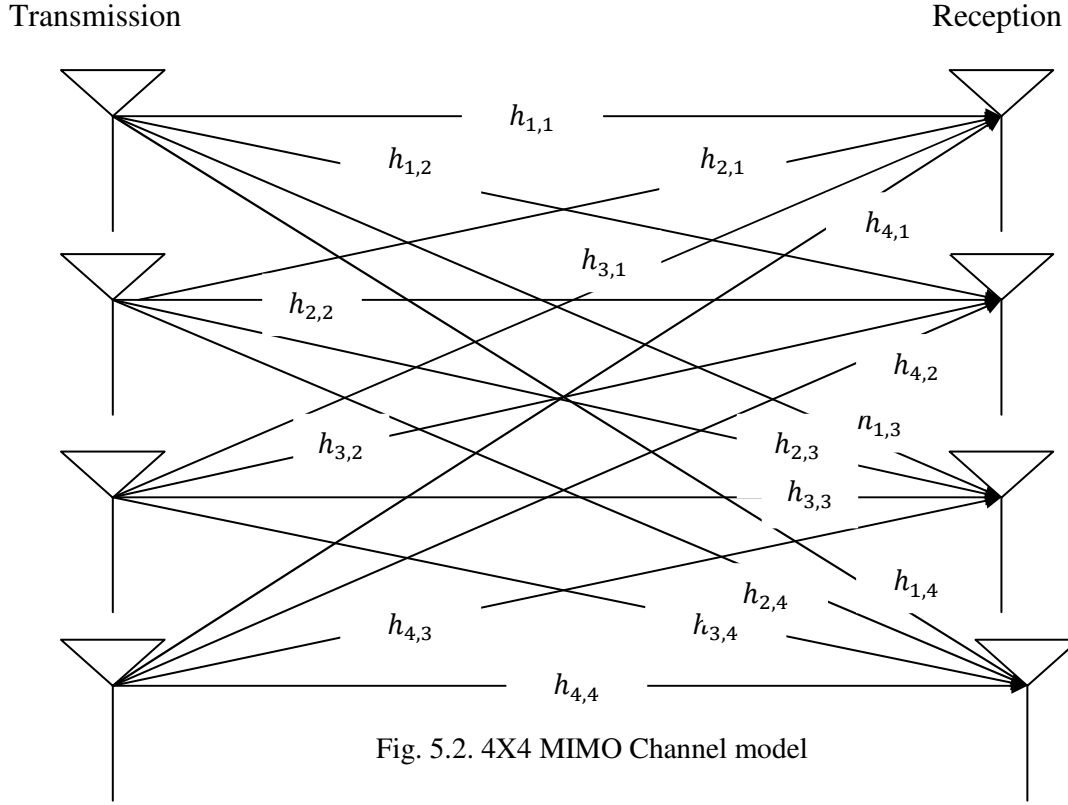
Fig. 5.2. 4X4 MIMO Channel model

The received signal for the 4×4 MIMO channel can be expressed as

$$y_j = \sum_{i=1}^{4} h_{j.i} x_i + n_j, \qquad j = 1, \ 2, \ 3, \ 4 \tag{5.9}$$

The above equation can be represented in matrix form as

$$\begin{bmatrix} y_1 \\ y_2 \\ y_3 \\ y_4 \end{bmatrix} = \begin{bmatrix} h_{1,1} & h_{1,2} & h_{1,3} & h_{1,4} \\ h_{2,1} & h_{2,2} & h_{2,3} & h_{2,4} \\ h_{3,1} & h_{3,2} & h_{3,3} & h_{3,4} \\ h_{4,1} & h_{4,2} & h_{4,3} & h_{4,4} \end{bmatrix} \begin{bmatrix} x_1 \\ x_2 \\ x_3 \\ x_4 \end{bmatrix} + \begin{bmatrix} n_1 \\ n_2 \\ n_3 \\ n_4 \end{bmatrix} \tag{5.10}$$

In the case of 4×4 MIMO, ML detection minimizes

$$J = \left\| \begin{bmatrix} y_1 \\ y_2 \\ y_3 \\ y_4 \end{bmatrix} - \begin{bmatrix} h_{1,1} & h_{1,2} & h_{1,3} & h_{1,4} \\ h_{2,1} & h_{2,2} & h_{2,3} & h_{2,4} \\ h_{3,1} & h_{3,2} & h_{3,3} & h_{3,4} \\ h_{4,1} & h_{4,2} & h_{4,3} & h_{4,4} \end{bmatrix} \begin{bmatrix} \hat{x_1} \\ \hat{x_2} \\ \hat{x_3} \\ \hat{x_4} \end{bmatrix} \right\|^2 \tag{5.11}$$

If the modulation is BPSK, the possible values of x_1 and x_2 are $+1$ or -1. So, to find the ML estimate, we need to find the minimum from the all sixteen combinations of x_1, x_2, x_3, x_4 with J defined for the sixteen combinations as

$$J_{+1,+1,+1,+1} = \left\| \begin{bmatrix} y_1 \\ y_2 \\ y_3 \\ y_4 \end{bmatrix} - \begin{bmatrix} h_{1,1} & h_{1,2} & h_{1,3} & h_{1,4} \\ h_{2,1} & h_{2,2} & h_{2,3} & h_{2,4} \\ h_{3,1} & h_{3,2} & h_{3,3} & h_{3,4} \\ h_{4,1} & h_{4,2} & h_{4,3} & h_{4,4} \end{bmatrix} \begin{bmatrix} +1 \\ +1 \\ +1 \\ +1 \end{bmatrix} \right\|^2$$

$$J_{+1,+1,+1,-1} = \left\| \begin{bmatrix} y_1 \\ y_2 \\ y_3 \\ y_4 \end{bmatrix} - \begin{bmatrix} h_{1,1} & h_{1,2} & h_{1,3} & h_{1,4} \\ h_{2,1} & h_{2,2} & h_{2,3} & h_{2,4} \\ h_{3,1} & h_{3,2} & h_{3,3} & h_{3,4} \\ h_{4,1} & h_{4,2} & h_{4,3} & h_{4,4} \end{bmatrix} \begin{bmatrix} +1 \\ +1 \\ +1 \\ -1 \end{bmatrix} \right\|^2$$

$$\vdots \tag{5.12}$$

$$J_{-1,-1,-1,+1} = \left\| \begin{bmatrix} y_1 \\ y_2 \\ y_3 \\ y_4 \end{bmatrix} - \begin{bmatrix} h_{1,1} & h_{1,2} & h_{1,3} & h_{1,4} \\ h_{2,1} & h_{2,2} & h_{2,3} & h_{2,4} \\ h_{3,1} & h_{3,2} & h_{3,3} & h_{3,4} \\ h_{4,1} & h_{4,2} & h_{4,3} & h_{4,4} \end{bmatrix} \begin{bmatrix} -1 \\ -1 \\ -1 \\ +1 \end{bmatrix} \right\|^2$$

$$J_{-1,-1,-1,-1} = \left\| \begin{bmatrix} y_1 \\ y_2 \\ y_3 \\ y_4 \end{bmatrix} - \begin{bmatrix} h_{1,1} & h_{1,2} & h_{1,3} & h_{1,4} \\ h_{2,1} & h_{2,2} & h_{2,3} & h_{2,4} \\ h_{3,1} & h_{3,2} & h_{3,3} & h_{3,4} \\ h_{4,1} & h_{4,2} & h_{4,3} & h_{4,4} \end{bmatrix} \begin{bmatrix} -1 \\ -1 \\ -1 \\ -1 \end{bmatrix} \right\|^2$$

5.3. Proposed scheme for transmission over Rayleigh fading channels

The schematic block diagram of the proposed transmission scheme is as shown in Figure 5.3. The transmitter side consists of a robust watermark embedding unit which has already been discussed in Chapter 2, a BPSK modulator unit to modulate the watermarked image, a serial to parallel conversion unit (S/P) and a transmitter with multiple antennas. At the receiver side, a receiver with multiple antennas, a ML MIMO detector and a parallel to serial conversion unit (P/S), a BPSK demodulator, and a watermark extracting unit perform in the reverse order to that at the transmitter.
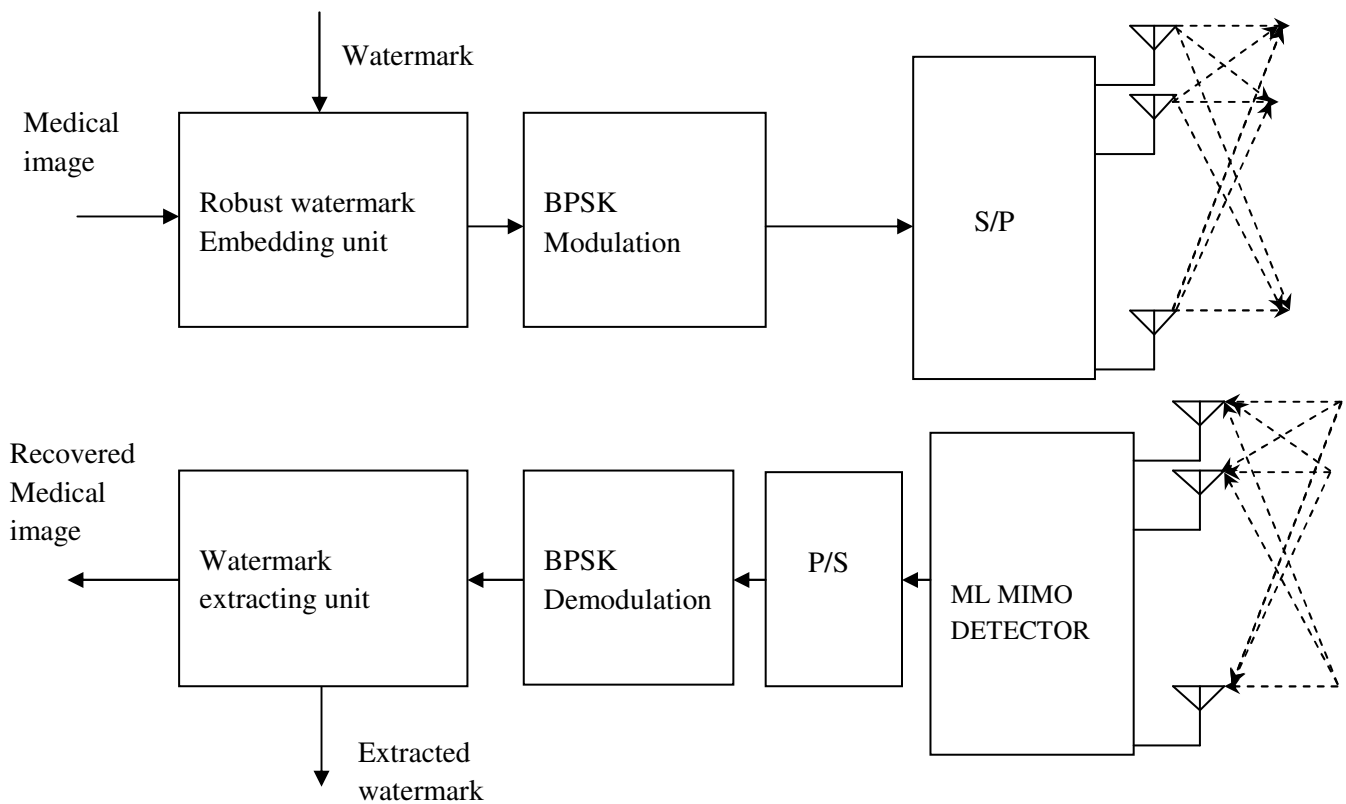

Fig. 5.3. The schematic block diagram of the proposed transmission scheme

5.4. Implementation of the proposed scheme

The scheme proposed in the previous section for transmission of watermarked medical images over a Rayleigh fading MIMO channel is implemented using MATLAB in order to study its performance. For this purpose we consider the same watermark (namely, the patient information) that was used for the SISO scheme in Chapter 4 and encrypt it using the algorithm explained in Section 3.2.3. For the sake of convenience, the patient information (text file) and the encrypted watermark are shown in Figures 5.4 (a) and 5.4(b), respectively. The medical image considered is an MRI gray image of size 250×192 with brain tumor. The encrypted watermark is now embedded in the MRI image using the embedding process described in Section 3.2.3. The watermark embedded MRI image with brain tumor (which appears as a white area at lower left side of the image) is shown in Figure 5.5. From Figure 5.5, it is clear that the embedding process does not affect the image quality. The watermarked MRI image is now transmitted over a Rayleigh fading SISO channel, or over a 2×2 MIMO channel or over a 4×4 MIMO channel in order to evaluate the performance over the various channels. BPSK modulation is used in this evaluation and channel information is assumed to be known at the receiver. The watermark extraction process implemented in the previous chapter is used here for watermark extraction. The bit error rate (BER) performance of the system is now evaluated for different signal to noise ratios (SNRs) E_b/N_0, where E_b is the energy received per bit and N_0 is the noise power spectral density. The BER performance of the proposed scheme for SISO, 2×2 MIMO, and 4×4 MIMO schemes are shown in Figure 5.6. From this figure, it is clear that the proposed 4x4 MIMO scheme outperforms the 2x2 MIMO and SISO schemes as far as the BER rate is concerned, for all values of SNRs.

In order to see the whether the watermark has been extracted exactly and to study the quality of the restored image, a value of $E_b/N_0 = 4\,dB$ is chosen. The restored MRI image and the extracted watermark when the watermarked image is transmitted over the SISO channel are shown in Figures 5.7 and 5.8, respectively. The corresponding results are shown in Figures 5.9 and 5.10, respectively when the watermarked image is transmitted over 2×2 MIMO channel. Finally, the restored MRI image and the extracted watermark are shown in Figures 5.11 and 5.12 respectively, the watermarked image is transmitted over 4×4 MIMO channel. From Figures 5.7 and 5.8, it is observed that the SISO scheme has neither restored the image well nor extracted the watermark correctly. The 2×2 MIMO scheme has extracted watermark exactly but not restored the image properly, as can be seen from Figures 5.10 and 5.9, respectively. However, the 4×4 MIMO scheme has restored the image and extracted the watermark exactly, as can be seen from Figures 5.11 and 5.12.

CARE

HYDERABAD

 PATIENT NAME: JOSEPH

  AGE: 45   (a)

BP: NO

BS: NO

¾ » Ò Á

Å Ú ¿ Á Ò » ¼ » ¿

Ð » Ô Æ Á Í Ô t Í » Ì Á ¯ È Î Ó ÁÐ »   (b)

 » Ä Á ¯ ¤ ¦

¼ Ð¯ Í Î

¼ Ó¯ Í Î
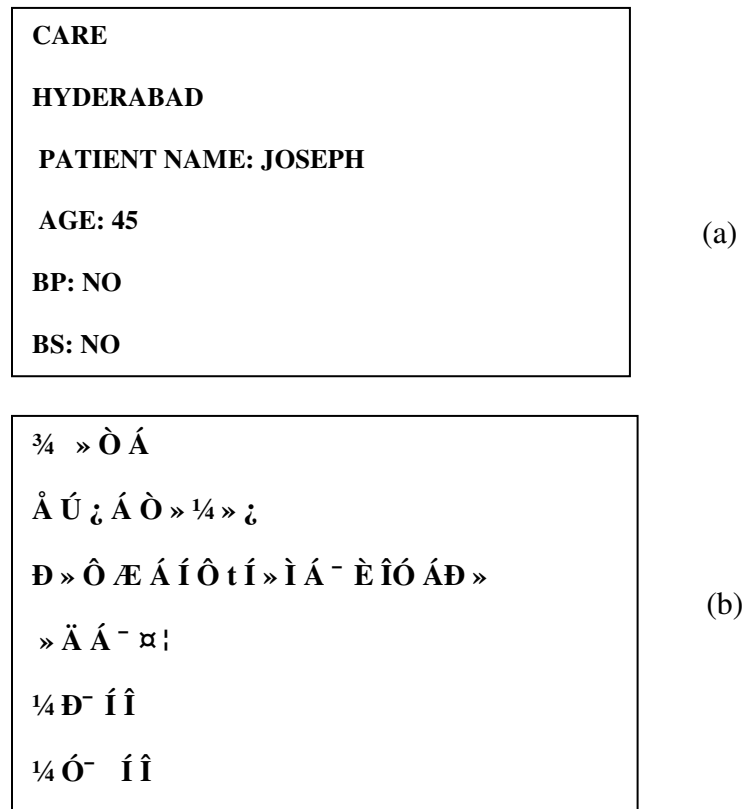
Fig. 5.4 (a) Watermark (b) encrypted watermark

Watermark embedded
region
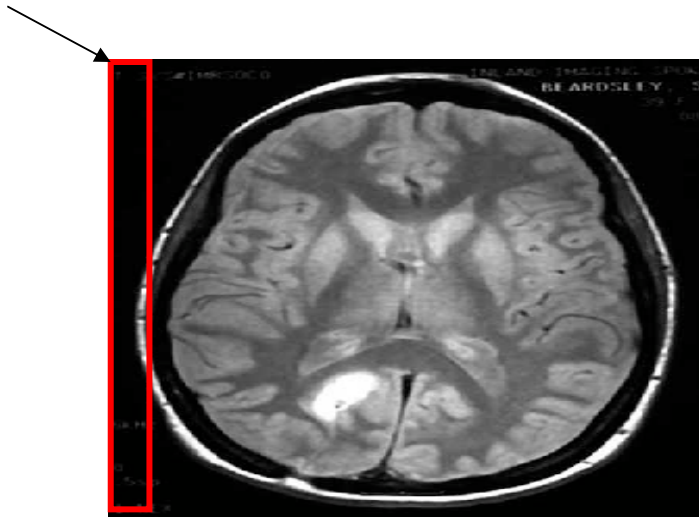
Fig. 5.5. Watermark embedded MRI brain image
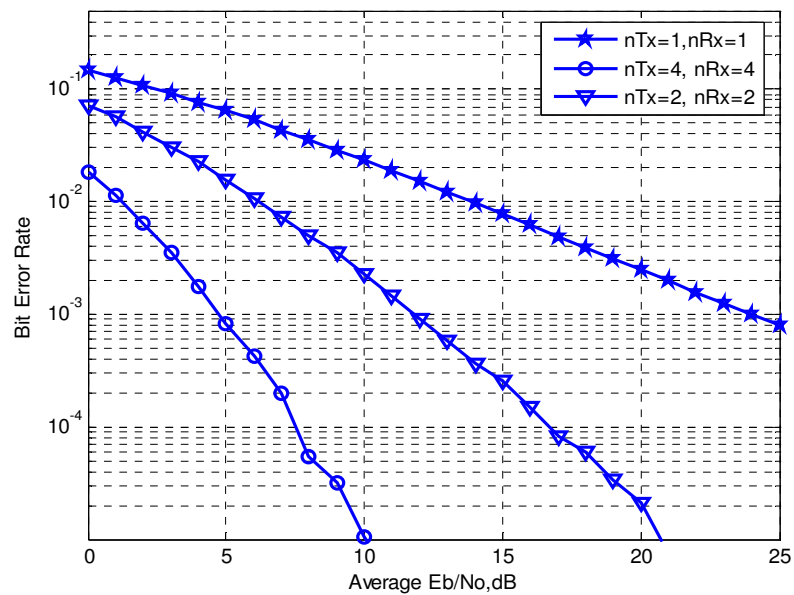
Fig. 5.6. BER performance of SISO, 2x2 MIMO and 4x4 MIMO Rayleigh fading
channels
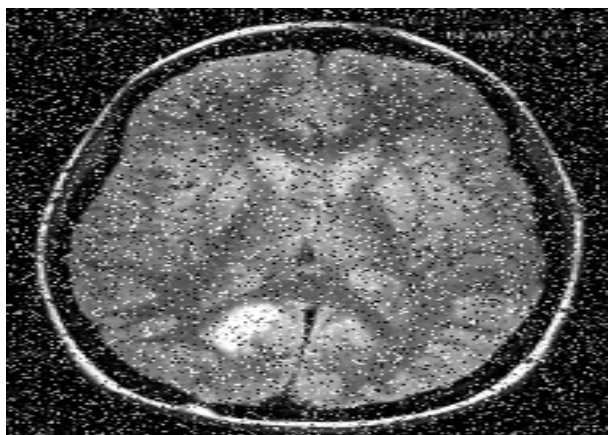
Fig. 5.7. Recovered MRI brain image with SISO scheme at $E_b/N_0 = 4dB$

Fig. 5.8. Extracted watermark with SISO scheme   at $E_b/N_0 = 4dB$
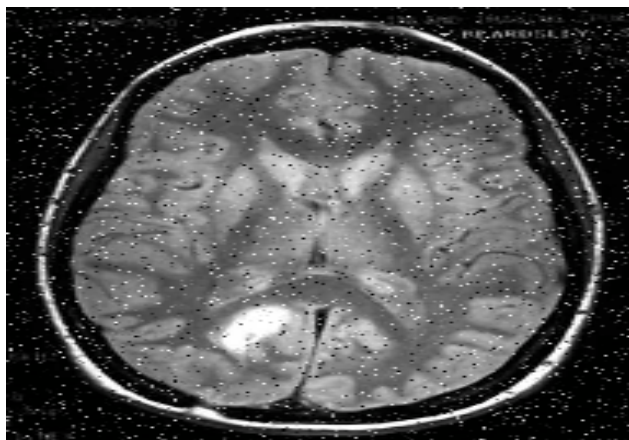
Fig. 5.9. Recovered MRI brain image with 2×2 MIMO scheme at $E_b/N_0 = 4dB$

CARE

HYDERABAD

 PATIENT NAME: JOSEPH

 AGE: 45

BP: NO

BS: NO

Fig. 5.10. Extracted watermark with 2×2 MIMO scheme at $E_b/N_0 = 4dB$
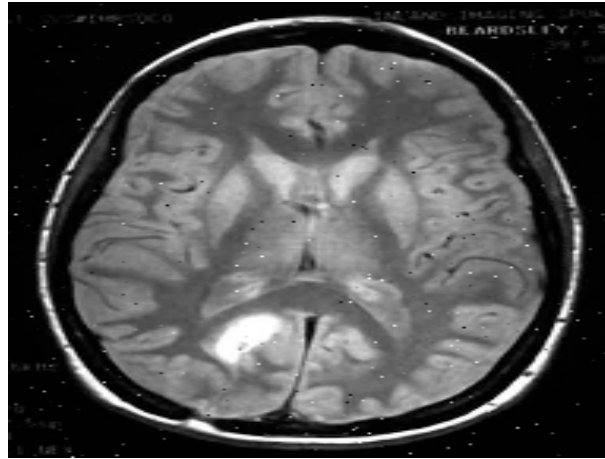
Fig. 5.11. Recovered MRI brain image with 4×4 MIMO scheme at $E_b/N_0 = 4dB$

CARE

HYDERABAD

 PATIENT NAME: JOSEPH

 AGE: 45

BP: NO

BS: NO

Fig. 5.12. Extracted watermark with 4×4 MIMO scheme at $E_b/N_0 = 4dB$

5.5. Conclusion

In this Chapter, we have proposed a scheme with MIMO channel for transmission of medical images over Rayleigh fading channels with concealed patient information as watermark and its performance analyzed using MIMO ML detector at the receiver. The proposed approach has been demonstrated by transmitting a watermarked MRI image with the patient information as watermark. From the results, it is clear that the proposed scheme can be used to advantage to transmit medical images with patient information concealed as watermark by using a 4×4 MIMO channel as opposed to a SISO channel or even a 2×2 MIMO channel.

CHAPTER 6

MIMO SFBC OFDM SCHEME FOR TRANSMISSION OF WATERMARKED MEDICAL IMAGES OVER RAYLEIGH FADING CHANNELS

In chapter 5, we proposed a MIMO scheme for transmission of watermarked medical images over Rayleigh fading channels. MIMO channel can mitigate the detrimental effects due to multipath fading, but it cannot reduce the effects due to frequency selective fading or potential multipath fading. In order to reduce the effect of frequency selective fading, we propose a new MIMO space-frequency block coded (SFBC) OFDM scheme for transmission of watermarked medical images over Rayleigh fading channels in this Chapter. The effectiveness of the proposed scheme is demonstrated through experimental results.

6.1. Introduction

With the advent of next generation broadband wireless communications, combination of MIMO wireless technology with OFDM has been recognized as one of the most promising techniques to support higher data rates and high performance. In particular, coding over the space, time, and frequency domains provided by MIMO-OFDM will enable much more reliable and robust transmission over the harsh wireless communication channels [11].

 In view of the bandwidth efficiency and immunity to multipath propagation over single carrier transmission, OFDM has been adopted in many digital communication standards. However, it does not possess any special immunity against severe frequency-selective channels. To overcome this problem, Alamouti space-time block codes (STBC) based, MIMO OFDM system has been

considered in [46-48]. However, the sensitivity of STBC-OFDM system to channel variation in time domain causes severe performance degradation due to the channel difference over the STBC block duration. As a remedy for this problem, space-frequency block codes (SFBC) [49] are preferred. As such, in this chapter, a MIMO SFBC OFDM system is designed for transmission of the watermarked image over Rayleigh fading channels and its performance analyzed.

The remainder of this chapter is organized as follows. We first give a brief description of the minimum mean square error (MMSE) detection and vertical-Bell laboratories layered space-time (V-BLAST) mechanism. Then, we propose a robust MIMO SFBC OFDM scheme for transmission of watermarked medical images over Rayleigh fading channels. Then, we proceed for the MIMO SFBC OFDM system design, and implementation of the proposed scheme. Finally, we draw our conclusion.

6.2. V-BLAST mechanism

If a wireless channel has rich multipath scattering, then it is capable of producing large capacities with a relatively low number of bit errors [50-52]. Various techniques have been developed to take advantage of this property including BLAST. This architecture combines the advantage of space division multiple access (SDMA) or space division multiplexing (SDM). SDM is inherent to a MIMO system because multiple antennas are being used to transmit data at the same frequency across the wireless channel. Multiple receive antennas are required to ensure error-free decoding, which is another inherent property of a MIMO system.

MIMO spatial multiplexing has two common encoding methods: horizontal encoding method and vertical encoding method. Each data stream is independently encoded and transmitted by

different antennas in the horizontal encoding method. The vertical encoding method uses a single encoder for spreading information across all antennas. V-BLAST technique utilizes the horizontal encoding method. The term "vertical", as mentioned, does not refer to the encoding method used, but it refers to the method in which the detection at the receiver is performed. The V-BLAST transmission mechanism is illustrated in Figure 6.1.
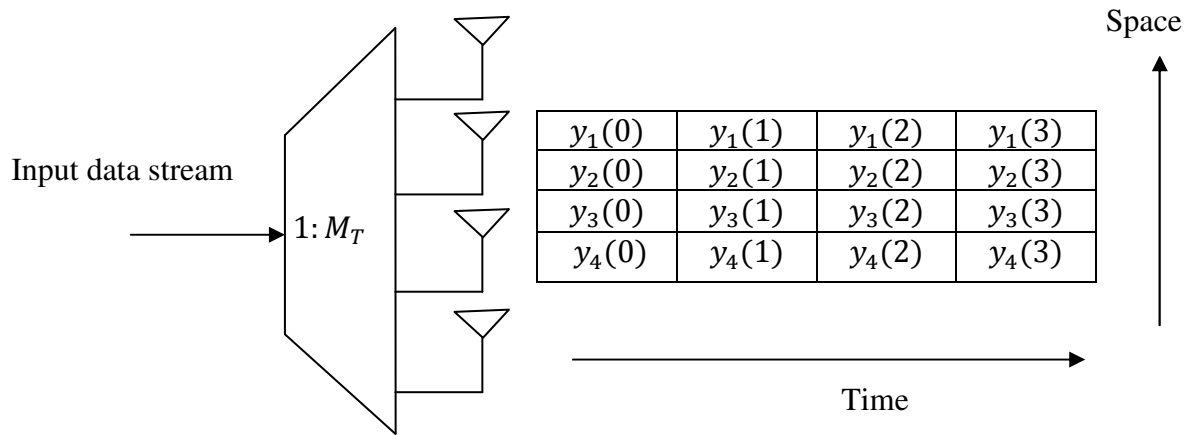
Fig. 6.1. V-BLAST Transmission Mechanism

As can be seen from Fig. 6.1, when the transmitted data stream is received, the initial received vector will consist of $y_i(0)$ where $i = 1, 2, 3, 4$, thus being vertically received. Due to the effect of multipath, the receivers will receive the signals radiated from all M_t transmit antennas. In comparison to other multiple access techniques, such as frequency division multiple access (FDMA), time division multiple access (TDMA), and code division multiple access (CDMA), V-BLAST ensures that the entire bandwidth of the system is used by all the transmitting antennas all the time, the entire bandwidth is occupied by each transmitted signal, and the total bandwidth utilized is only a small fraction in excess of the symbol rate [52].

At the receiver, V-BLAST requires its operation to be conducted in a multipath environment to achieve a sufficient level of de-correlation. These conditions allow the receiver to distinguish signals occupying the same channel space. To achieve a high rate of data transmission, V-BLAST and OFDM can be combined in frequency selective fading channels [53].

6.3. Proposed scheme

The schematic block diagram of the proposed scheme is illustrated in Figure 6.2. The transmitter side consists of a robust watermark embedding unit which has already been discussed in Chapter 2, a BPSK modulator unit to modulate the watermarked image, a serial to parallel conversion unit (S/P), an SFBC encoder and a MIMO OFDM unit. At the receiver side, an SFBC decoder, a MIMO OFDM de-multiplexing unit, and a parallel to serial conversion unit (P/S), a BPSK demodulator, and a watermark extracting process perform in reverse order to that at the transmitter.
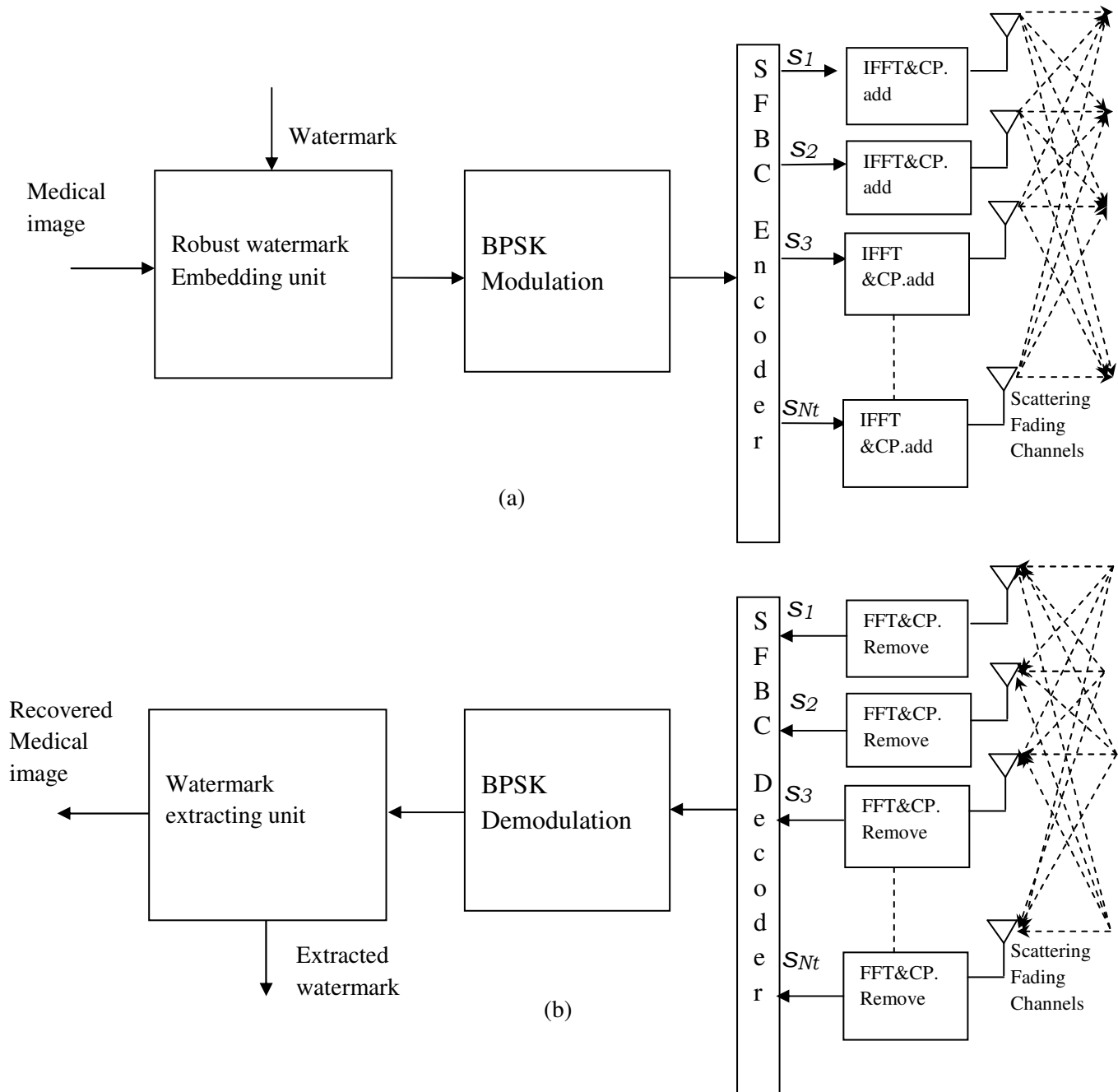
Fig. 6.2.The schematic block diagram of the proposed transmission system a) transmitter b) receiver

(i) MIMO SFBC OFDM System design

Assume that the system transmits data symbols $s_0, s_1, \ldots, s_K, s_{K+1}, \ldots, s_{N-1}$ on carriers 0, 1, $\ldots, K, K+1, \ldots, N-1$, respectively. In a SFBC-OFDM system, with two transmit antennas Tx1 and Tx2, pairs of information symbols are fed to the SFBC encoder as follows:

$$\begin{array}{cc} & \text{Tx1} \quad \text{Tx2} \\ \begin{array}{c} f_K \\ f_{K+1} \end{array} & \begin{bmatrix} s_K & s_{K+1} \\ -s_{K+1}^* & s_K^* \end{bmatrix} \end{array} \tag{6.1}$$

where s_{K+1}^* and s_K^* are the complex conjugates of s_{K+1} and s_K. The channel between Tx and Rx antennas is as shown in Figure 6.3. Let R_K^1 and R_K^2 be the received signals at the receive antennas Rx1 and Rx2, respectively for the kth carrier.
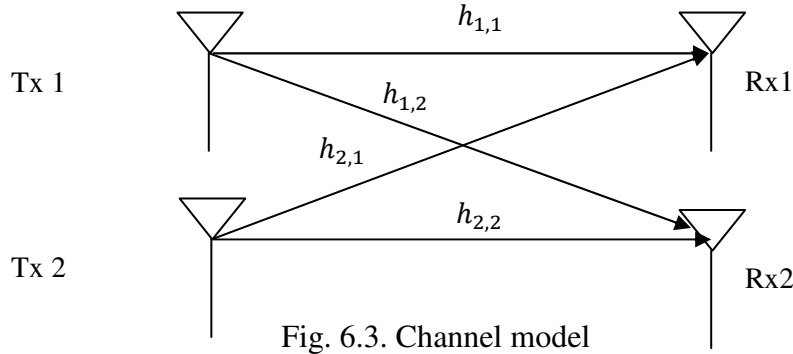
Fig. 6.3. Channel model

Let us denote the OFDM symbols by vector x obtained after the N-point inverse Fourier transform operation on the SFBC encoded data symbols. Assuming the cyclic prefix length to be greater than or equal to the channel impulse response length, and after removing the cyclic prefix, the received signals in the time domain can be expresses as

$$r = H_t x + \eta_t \tag{6.2}$$

where H_t the time-domain channel matrix and η_t is the time-domain additive white Gaussian noise vector. The received signals in the frequency domain are expressed as,

$$R = \begin{bmatrix} R_K^1 \\ R_{K+1}^{1^*} \\ R_K^2 \\ R_{K+1}^{2^*} \end{bmatrix} = HS + \eta = \begin{bmatrix} H_K^{11} & H_K^{21} \\ H_{K+1}^{21^*} & -H_{K+1}^{11^*} \\ H_K^{12} & H_K^{22} \\ H_{K+1}^{22^*} & -H_{K+1}^{12^*} \end{bmatrix} \begin{bmatrix} S_K \\ S_{K+1} \end{bmatrix} + \begin{bmatrix} \eta_K^1 \\ \eta_{K+1}^{1^*} \\ \eta_K^2 \\ \eta_{K+1}^{2^*} \end{bmatrix} \tag{6.3}$$

where R represents the received signals in the frequency domain, H is the frequency-domain channel matrix and η is the frequency-domain noise vector. Assuming that two adjacent carriers have the same channel characteristic, we have

$$H_K^{11} = H_{K+1}^{11} = H^{11}, \qquad H_K^{21} = H_{K+1}^{21} = H^{21} \tag{6.4}$$

$$H_K^{12} = H_{K+1}^{12} = H^{12}, \qquad H_K^{22} = H_{K+1}^{22} = H^{22}$$

Now, using per-tone V-BLAST MMSE detector [66], the estimate of data symbols $S^\wedge$ can be written as

$$S^\wedge = \begin{bmatrix} S_K^\wedge \\ S_{K+1}^\wedge \end{bmatrix} = H^H R = \begin{bmatrix} H^{11^*} & H^{21} & H^{12^*} & H^{22} \\ H^{21^*} & -H^{11} & H^{22^*} & -H^{12} \end{bmatrix} \begin{bmatrix} R_K^1 \\ R_{K+1}^{1^*} \\ R_K^2 \\ R_{K+1}^{2^*} \end{bmatrix} \tag{6.5}$$

6.4. Implementation of the proposed scheme

The scheme proposed in the previous section for transmission of watermarked medical images over Rayleigh fading channels is implemented using MATLAB to analyze its performance. For this purpose we consider two watermarks: (i) brain tumor patient information used for SISO scheme in Chapter 4 as Watermark 1 and kidney patient information (text file) as Watermark 2. The watermarks are shown in Figures 6.4 (a) and 6.5 (a), respectively. The watermarks are

encrypted using the algorithm discussed in Section 3.2.3. The encrypted watermarks are shown in Figures 6.4 (b) and 6.5 (b), respectively. The encrypted Watermark 1 is now embedded in the MRI image using embedded process described in Section 3.2.3. The watermark embedded MRI gray scale image of size 500×383 with brain tumor (which appears as a white area at lower left side of the image) is shown in Figure 6.6. The encrypted Watermark 2 is now embedded in the CT image. The watermark embedded CT gray scale image of the abdomen of a kidney patient is shown in Figure 6.7. From Figures 6.6 and 6.7, it is clear that the embedded process does not degrade the quality of the image. The watermarked medical images are now transmitted through a SISO-OFDM scheme or through a MIMO SFBC OFDM scheme. BPSK modulation technique is used in this evaluation and knowledge of the channel is assumed to be known at the receiver. The watermark extraction process implemented in Chapter 4 is used here for the watermark extraction. The BER performance of the system is now evaluated for different signal-to-noise ratios E_b/N_0. The BER performance of the SISO-OFDM and MIMO SFBC OFDM schemes are shown in Figure 6.8. From this figure, it is clear that the proposed MIMO SFBC OFDM scheme outperforms that of the SISO-OFDM scheme.

In order to see whether the watermark has been extracted exactly, and to study the restored image quality, values of $E_b/N_0 = 2dB \ and \ 4dB$ are chosen. The restored MRI image and the extracted watermark at $E_b/N_0 = 2 \ dB$ with SISO OFDM are shown in Figures 6.9 (a), 6.9 (b), respectively and the corresponding results at $E_b/N_0 = 4 \ dB$ are shown in Figures 6.10 (a) and 6.10 (b), respectively. The restored image with the proposed MIMO SFBC-OFDM system (two transmit and two receive antennas) at $E_b/N_0 = 4dB$ is shown in Figure 6.11. The extracted watermark with the proposed MIMO SFBC OFDM at $E_b/N_0 = 4dB$ is the same as the extracted watermark at $E_b/N_0 = 4dB$ with SISO OFDM.

The restored CT image and the extracted watermark at $E_b/N_0 = 2\,dB$ with MIMO SFBC-OFDM system (two transmit and two receive antennas) are shown in Figures 6.12 (a) and 6.12 (b) respectively, while the restored image with the proposed MIMO SFBC-OFDM system (two transmit and two receive antennas) at $E_b/N_0 = 4dB$ is shown in Figure 6.13. The extracted Watermark 2 with the proposed MIMO SFBC OFDM at $E_b/N_0 = 4dB$ is the same as the extracted watermark at $E_b/N_0 = 2\,dB$ with the proposed system. A comparison of the performance of SISO OFDM and the proposed MIMO SFBC OFDM at $E_b/N_0 = 2\,dB$ and $E_b/N_0 = 4dB$ is summarized in Table 6.1. From Table 6.1, it is observed that the proposed MIMO SFBC OFDM has restored the MRI and CT images as well as the watermarks properly at $E_b/N_0 = 4dB$. From these results, it is clear that the proposed MIMO SFBC OFDM outperforms the SISO OFDM for watermarked medical image transmission over Rayleigh fading channels.

CARE

HYDERABAD

 PATIENT NAME: JOSEPH

 AGE: 45   (a)

BP: NO

BS: NO

¾ » Ò Á

Å Ú ¿ Á Ò » ¼ » ¿

Ð » Ô Æ Á Í Ô t Í » Ì Á ¯ È Î Ó ÁÐ »

 » Ä Á ¯ ¤ ¦   (b)

¼ Ð¯ Í Î

¼ Ó¯ Í Î
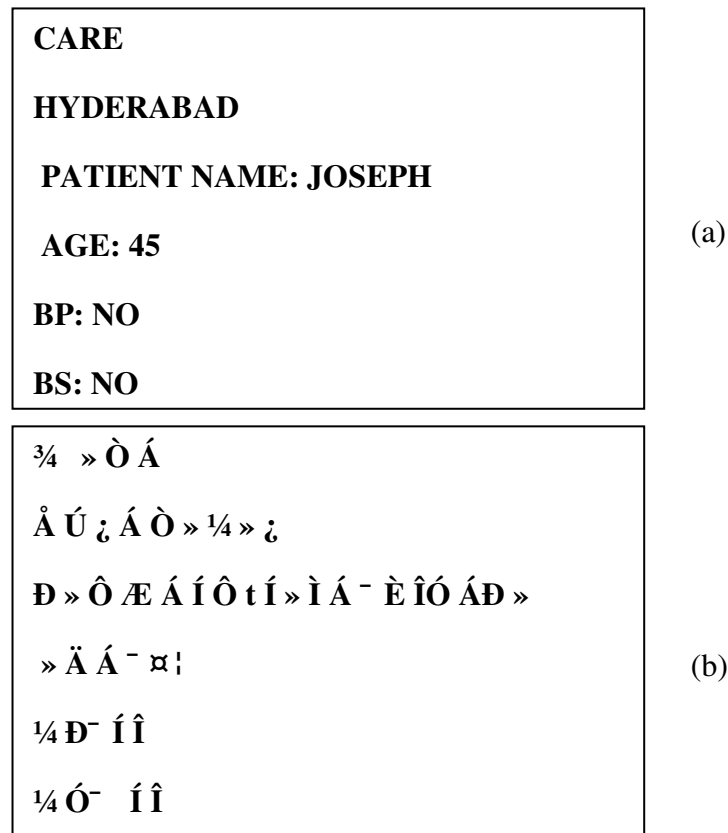
Fig. 6.4 (a) Watermark 1 (b) encrypted Watermark 1

KIMS

HYDERABAD

 PATIENT NAME: RANGAN

 AGE: 55

UMR NO: 93

(a)

É Æ Ì Ó

 Å Ú¿ Á Ò»¼»¿

 Ð» Ô Æ Á Í Ô t Í» Ì Á¯ Ò» Í Ä» Í

» Ä Á¯ ¦¦

Ö Ì Ò t Í Î̄ ¡®¢

(b)

Fig. 6.5 (a) Watermark 2 (b) encrypted Watermark 2
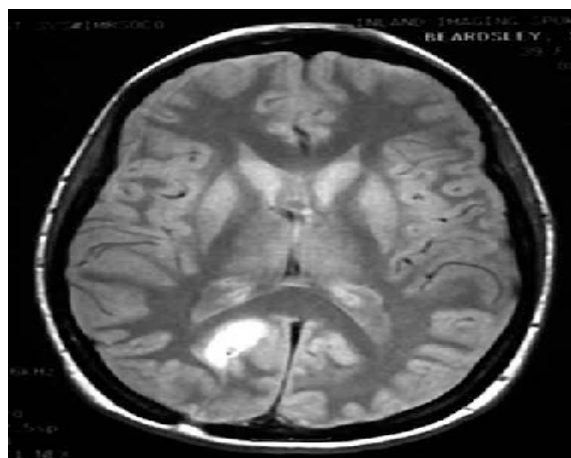
Fig. 6.6. MRI brain image embedded with encrypted Watermark1

Fig. 6.7. CT image of abdomen of a kidney patient embedded with encrypted
Watermark 2
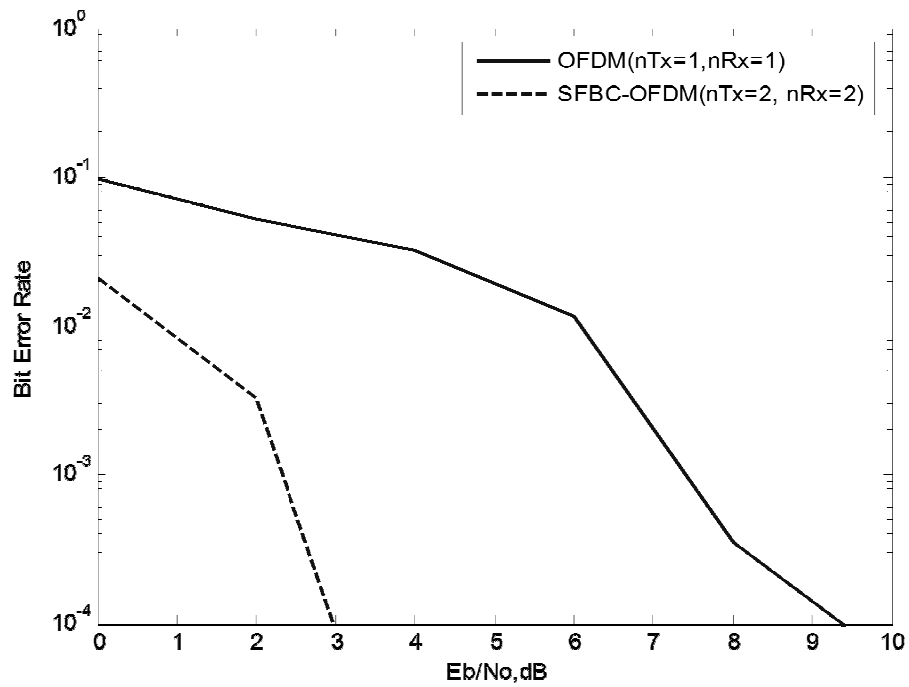
Fig. 6.8. BER Performance of OFDM and SFBC-OFDM
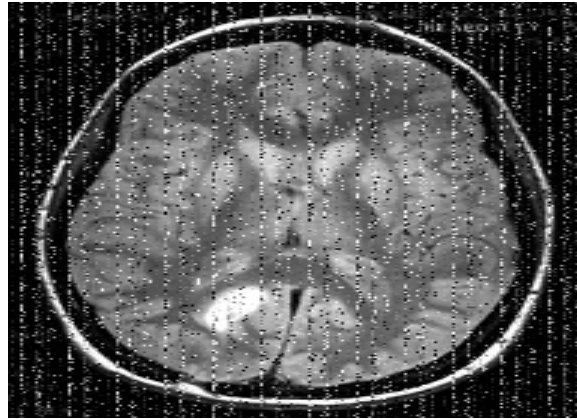
(a)

D 8 Z E

L Y? Q Y A=<D

 PATIENT NAME: JOSEPH

AGE: 45

BP: NO

BS: NO

(b)

Fig. 6.9 (a) Recovered MRI brain image and (b) extracted Watermark 1, with SISO OFDM scheme at $E_b/N_0 = 2\ dB$
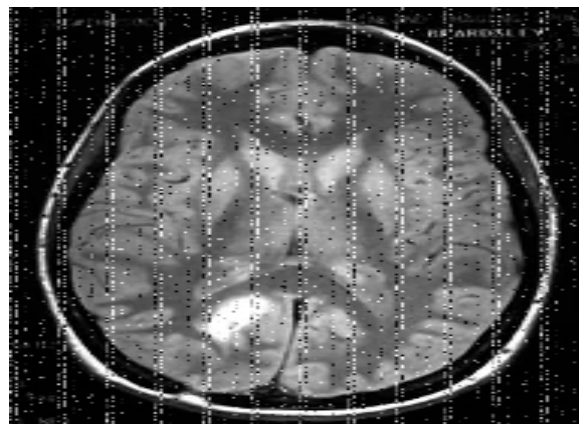
(a)

CARE

HYDERABAD

 PATIENT NAME: JOSEPH

AGE: 45

BP: NO

BS: NO

(b)

Fig. 6.10 (a) Recovered MRI brain image with SISO OFDM scheme at $E_b/N_0 = 4\ dB$
(b) extracted Watermark 1 with SISO OFDM scheme and 2×2 MIMO SFBC
OFDM at $E_b/N_0 = 4\ dB$
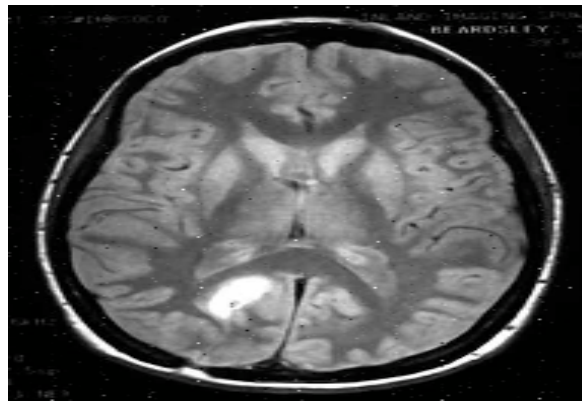
Fig. 6.11. Recovered MRI brain image using 2×2 MIMO SFBC OFDM scheme at
$E_b/N_0 = 4\ dB$

(a)

KIMS

HYDERABAD

 PATIENT NAME: RANGAN

 AGE: 55

UMR NO: 93

(b)

Fig. 6.12 (a) Recovered abdomen CT image using 2×2 MIMO SFBC OFDM scheme at $E_b/N_0 = 4 \, dB$ (b) extracted Watermark 2, using 2×2 MIMO SFBC OFDM scheme at $E_b/N_0 = 2 \, dB, \ 4dB$

Fig. 6.13. Recovered abdomen CT image using 2×2 MIMO SFBC OFDM scheme at $E_b/N_0 = 4 \, dB$

Table 6.1: Performance comparison of SISO OFDM and MIMO SFBC OFDM

Images	E_b/N_0	SISO OFDM		MIMO SFBC OFDM	
		Image	Watermark	Image	Watermark
MRI	$2dB$	Not Restored	Not Restored	Not Restored	Restored
	$4dB$	Not Restored	Restored	Restored	Restored
CT	$2dB$	Not Restored	Not Restored	Not Restored	Restored
	$4dB$	Not Restored	Restored	Restored	Restored

6.5. Conclusion

In this chapter, we have proposed a MIMO SFBC OFDM scheme for transmission of medical images over Rayleigh fading channels and its performance analyzed in comparison with SISO-OFDM using MMSE V-BLAST based detection at the receiver. The proposed approach has been demonstrated by transmitting watermarked medical images with the patient information as the watermark. From the results, it is clear that the proposed MIMO SFBC OFDM scheme can be used to advantage to transmit medical images with patient information concealed as watermark as opposed to the SISO-OFDM.

CHAPTER 7

PERFORMANCE COMPARISON OF THE PROPOSED

SCHEMES

In the previous chapters, we have proposed three schemes for transmission of watermarked medical images over fading channels. In Chapter 4, we proposed a scheme for transmission of watermarked medical images over an SISO channel. In Chapter 5, we introduced a scheme for transmission of watermarked medical images over a MIMO Rayleigh fading channel. In Chapter 6, we presented a MIMO SFBC OFDM scheme for transmission of medical images over Rayleigh fading channels. In this chapter, we compare the performance of the three proposed schemes.

The basic measure of performance is the capacity of a channel: the maximum rate of communication for which arbitrarily small error probability can be achieved. In Chapter 2, we discussed the capacities of SISO and MIMO channels. The total capacity of the MIMO channel is made up by the sum of parallel SISO sub-channels. So MIMO channel capacity is very high and it produces higher transmission data rates. Due to its limited channel capacity, SISO channel is not suitable for the modern wireless services. As mentioned in the previous chapters, ML detection shows a better performance in terms of minimizing the overall probability compared to V-BLAST, ZF, and MMSE detection, but the complexity is very high. V-BLAST MMSE detection complexity is very much less compared that of turbo and ML. A comparison of the proposed three schemes is summarized in Table 7.1.

In order to study the performance of the proposed schemes, simulations were carried out at various SNRs. A comparison of the performance of SISO scheme, MIMO scheme and MIMO

SFBC OFDM at $E_b/N_0 = 2\ dB$ and $E_b/N_0 = 4dB$ is summarized in Table 7.2. It is seen from this table that all the three schemes are able to recover the image well and extract the watermark properly at $SNR = 4dB$. It is also observed that none of the schemes is able to recover the image well when $SNR = 2dB$ and that it is only the 2×2 MIMO SFBC OFDM scheme with V-BLAST MMSE detection that is able to extract the watermark properly at $SNR = 2dB$. From the implementation results, it is clear that the 2×2 MIMO SFBC OFDM scheme outperforms the SISO scheme and MIMO scheme.

Table 7.1: Comparison of proposed schemes

	Proposed scheme 1	Proposed scheme 2	Proposed scheme 3
Scheme	Watermarked medical image transmission over an SISO channel	Watermarked medical image transmission over a MIMO Rayleigh fading channel	Watermarked medical image transmission over Rayleigh fading channels using MIMO SFBC OFDM
Channel capacity	SISO channel capacity is very less	MIMO channel capacity high (a sum of many parallel SISO channels)	Channel capacity is high
Detection technique	Turbo decoding (iterative soft decoding)	Maximum likelihood (ML)	V-BLAST MMSE
Advantages	(i) Reduces the impulsive noise effect	(i) MIMO channels are very high capacity channels. So it provides the higher data rates. (ii) MIMO can mitigate the detrimental effects due to multipath fading.	(i) MIMO can improve the capacity and the diversity and OFDM can mitigate the detrimental effects due to potential multipath fading.
Disadvantages	(i) SISO channel provides less data rate due to less capacity and not reliable due to multipath fading. (ii) Decoding complexity is very high.	(i) MIMO could not mitigate the detrimental effects due to frequency selective fading. (ii) ML decoding complexity is high	(i) Practical approach to implementation of this system is highly complex.

Table 7.2: Performance comparison of SISO scheme, MIMO scheme and MIMO SFBC OFDM scheme

Image	E_b/N_0	SISO scheme		MIMO scheme (4×4)		(2×2) MIMO SFBC OFDM scheme	
		Image	Watermark	Image	Watermark	Image	Watermark
MRI	$2dB$	Not Restored	Not Restored	Not Restored	Not Restored	Not Restored	Restored
	$4dB$	Restored	Restored	Restored	Restored	Restored	Restored

CHAPTER 8

CONCLUSIONS AND FUTURE WORKS

8.1. Conclusions

This thesis has been concerned with the development of different schemes for watermarked medical image transmission over fading channels and analysis of their performances through simulations.

Transmitting separately a large amount of information as word documents and medical images through media like the internet may cause excessive memory utilization and transmission overheads. In order to remove these transmission overheads, we have proposed a medical watermarking scheme, that takes into account both memory utilization and security. This approach has been used in all the proposed schemes for digital watermarking in this thesis.

As a first scheme, we have proposed a robust approach for transmission of medical images over impulsive wireless noisy channels. However, wireless channels have fluctuating characteristics, and hence, data transmission errors can occur during image transmission. To correct the transmission errors, we have used turbo channel coding in the scheme. The proposed approach has been illustrated through implementation results of transmitting a watermarked medical image in Chapter 4. In this scheme, we have used a single-input single-output (SISO) channel, but such a channel has limited capacity. Modern wireless services require reliable wireless channels with large capacities. Further, SISO channel is not reliable due to multipath fading.

In order to overcome the above problems, we have introduced a second scheme. In the second scheme, we have used a multi-input multi-output (MIMO) system for transmission of medical images over Rayleigh fading channels with concealed patient information as the watermark and its performance has been analyzed using MIMO ML detector at the receiver. MIMO channels have large capacity and are very effective against channel flat fading. Simulation results have been provided in Chapter 5 to demonstrate the effectiveness of transmitting watermarked data over this medium of transmission.

We have proposed yet another scheme called MIMO space-frequency block coded (SFBC) OFDM for transmission of watermarked medical images over Rayleigh frequency selective fading channels and have analyzed its performance in comparison with that of transmitting the same over a SISO-OFDM system, using V-BLAST based MMSE detection at the receiver. The efficacy of the proposed scheme has been illustrated through implementation results on two watermarked medical images in Chapter 6.

We have concluded that the MIMO based transmission schemes are more effective for transmission of watermarked medical images on fading channels at low signal-to-noise ratios.

8.2. Suggestions for Future Work

Based on the results obtained in this thesis, the following problems are worth pursuing.

- **Cooperative OFDM**

It is well-known that space-time coding can be applied to both co-operative systems and MIMO systems, to achieve spatial diversity, where multiple transmissions are received at the receiver. A major difference between the MIMO and cooperative systems is that multiple transmissions from

relay nodes in a cooperative system may not be well synchronized and a space-time code achieving spatial diversity for an MIMO system may not do well in a cooperative system. This issue has been studied lately in [54-63], where there are two major approaches. The first approach is based on time domain considerations [54-57], while the second on frequency domain considerations [58-63]. The idea in the approach is to treat the paths from the relay nodes to the destination node as multi-paths and then to combat the time delays, use OFDM transmissions at relay nodes, and then space-time/frequency coding for achieving the multipath (cooperative spatial in this case) diversity. To improve the performance of the OFDM, the fundamental concept of the cooperative diversity can be applied on the OFDM. It is a more practical approach to implement communication applications such as image and data transmission. Combination of cooperative and MIMO systems is already providing high data rates with high quality of modern wireless services. By taking advantage of this, new schemes could be developed for data or image transmission over fading channels to produce better results.

- **MIMO-OWDM**

In the wavelet domain, sub-band components can be separated in the same way that OFDM does, and is called orthogonal wavelet division multiplexing (OWDM). The major difference between OFDM and OWDM is that in OFDM, we use FFT which performs sub-band decomposition with a specific number of sub-bands at well defined intervals, whereas in OWDM, it is possible to dynamically allocate the number of sub-bands as well as the bandwidth. Of course, if there are sufficient levels, the OWDM would start to resemble the OFDM Symbol. With OWDM, It is possible to perform the multiplexing at the input to the OWDM block meaning that the technology at the consumer end would become significantly less complex (although it would be more complex at the transmitter).

The complexity of an OFDM system is very greater than that of an OWDM system. OFDM systems require large FFTs, whereas OWDM systems require only a number of low-order filters (2nd order in the case of the Haar filter). DWT has a complexity of $O(N)$ as opposed to a complexity of $O(Nlog_2(N))$ for the FFTs. Implementation cost of OFDM is higher than that of OWDM. The advantages of MIMO have already been discussed in the thesis. A combination of MIMO-OWDM will simply perform like a MIMO-OFDM does, but with less complexity. It would be worthwhile proposing a MIMO-OWDM scheme for image transmission.

- **STF-coded OFDM**

The performance of space-time frequency (STF) codes in MIMO-OFDM systems has also been studied recently for a variety of system configurations and channel conditions in [64]. It has been shown that the maximum diversity is a product of time, frequency, and space diversities [65]. Performance analysis of robust image transmission with STF-coded OFDM in comparison with SF-coded OFDM and ST-coded OFDM would be a valuable addition to the work contained in this thesis.

REFERENCES

[1] B. M. Irany, X. C. Guo and D. Hatzinakos, "A high capacity reversible multiple watermarking scheme for medical Image," *Proceedings of the IEEE International Conference on DSP*, *Corfu*, Greece, pp. 1-6, Jul. 2011.

[2] Z. Chang and J. Xu, "Reversible run length data embedding for medical Images," *Proceedings of the IEEE 3rd International Conference on Communication Software and Networks (ICCSN), Xi'an,* China, pp. 260-263, May 2011.

[3] U. R. Acharya, D. Anand, P. S. Bhat, and U. C. Niranjan, "Compact storage of medical images with patient information," *IEEE Trans. Information Technology in Bio-medicine,* vol. 5, no. 4, pp. 320-323. Dec. 2001.

[4] J. Kivijarvi, T. Ojala, T. Kaukoranta, A. Kuba, L. Nyul, and O. Nevalainen, "A comparison of lossless compression methods for medical images," *Compute Med Imaging Graph*, vol. 22, no. 4, pp. 323-339, Jul. 1998.

[5] E. Reiter, "Wavelet compression of medical Imagery," *Telemed Journal*, vol. 2, no. 2, pp. 131-137, Aug. 1996.

[6] S. Hyakin, "Communication systems," *Fourth edition, John Wiley & Sons, New Delhi,* India, 2010.

[7] K. Khatir "Coded cooperative communications," *M. S. thesis, Blekinge Institute of Technology, Karlskrona, Sweden,* Sep. 2007.

[8] T. S. Rappaport "Wireless communications principles and practice," *second edition, Printice Hall, Upper Saddle River, New Jersey,* USA, 2002.

[9]   K. L. Du, M. N. S. Swamy, "Wireless communication systems: From RF subsystems to 4G enabling technologies," *Cambridge University Press*, *New york,* USA, 2010.

[10] M. K. Simon & M. S. Alouini, "Digital communications over fading channles," *second edition, John Wiley& Sons, New york,* USA, 2005.

[11] W. Zhang, X. G. Xia, K. B. Letaief, "Space-time/frequency coding for MIMO-OFDM in next generationbroad band wireless systems," *IEEE Trans. Wireless Communications*, pp. 32-43, Jun. 2007.

[12] M. Janikiraman,"Space-time codes and MIMO systems," *Artech House universal personal communications series*, *Boston,* USA, 2004.

[13] S. M. Alamouti, "A simple transmit diversity technique for wireless communication," *IEEE journal. Selected areas in communication,* vol. 16, no. 8, pp. 1451–58, Oct. 1998.

[14] H. D. Saglam, "Simulation performance of multiple input multiple output systems employing single carrier modulation and orthogonalfrequency division multiplexing," *M. S. thesis, Naval post graduate school, Montery*, Calfornia, USA, Dec. 2004.

[15] G. Rayleigh, J. Cioffi, "Spatio-temporal coding for wireless communications," *IEEE Trans. Communications,* vol. 46, no. 3, pp. 357-366, Mar. 1998.

[16] J. R. Barry, E. A. Lee, D. G. Messerschmitt, "Digital communications", *Kluwer Academic Publishers, Massachusetts*, USA, 2004.

[17] V. Tarokh, N. Seshadri, R. A. Calderbank, "Space-time codes for higher data rate wireless communication: Performance criterion and code construction," *IEEE Trans. Information Theory,* vol.44, no. 2, pp.744-765, Mar. 1998.

[18] G. B. Giannakis, Z. Liu, X. Ma, S. Zhou, "Space-time coding for broadband wireless communications," *John Wiley& Sons, New Jersy,* USA, 2007.

[19] S. Sanayei, A. Hedayat, and A. Nosratinia, "Space-time codes in key hole channels:analysis and design," *IEEE Trans. Wireless Communications*, vol. 6, no. 6, pp. 2006-2011, Jun. 2007.

[20] K. F. Lee and D. B. Williams, "A space-frequency transmitter diversity technique for OFDM systems," *Proceedings of the IEEE Global Communications Conference,* vol. 3, pp. 1473–77, Nov. 2000.

[21] E. E. A Abdallah, "Robust digital watermarking techniques for multimedia protection", *Ph.d thesis, Concordia University, Montreal, QC,* Canada, Mar. 2009.

[22] D. Mistry, "Comparison of digital watermarking methods," *International jouranal. Computer Sceince and Engineering*, vol. 2, no. 9, pp. 2905- 2909, Dec. 2010.

[23] G. Coatrieux, H. Maitre, B. Sankur, B. Rolland and R. Collorec, "Relevance of watermarking in medical imaging", *Proceedings of 3rd Conference Information Technology Application in Biomedicine, ITAB, Airlington,* USA, pp. 250-255, Nov. 2000.

[24] E. T. Lin and E. J. Delp, "A Review of Fragile Image Watermarks," *Proceedings of the Multimedia and Security Workshop on Multimedia Contents*, *Orlando, Florida,* USA, pp. 25-29, October 1999.

[25] J. Fridrich, "A hybrid watermark for tamper detection in digital images," *Proceedings of the Fifth International Symposium on Signal Processing and Its Applications*, vol. 1, pp.301-304, Aug. 1999.

[26] E. T. Lin and E. J. Delp, "A Review of Data Hiding in Digital Images", *Proceedings of the Image Processing, Image Quality, Image Capture Systems Conference* (PICS'99) pp. 274—278, Jun. 1999.

[27] J. Nayak, P. S. Bhat, M. S. Kumar , and R. Acharya, "Reliable and robust transmission and storage of medical images with patient information," *International Conference on Signal Processing and Communications (SPCOM),* pp.91-95, Dec. 2004.

[28] W. E. Ryan, S. Lin "Channel codes classical and modern," *Cambridge University Press, New York,* USA, 2009.

[29] E. Biglieri "Coding for wireless channels," *Springer international edition, New york,* USA, 2005.

[30] C. E. Shannon, "A mathematical theory of communication," *The Bell system technical journel*, vol. 27, pp. 379-423, Jul. 1948.

[31] C. Berrou and A. Glavieux , "Near optimum error correcting coding and decoding: turbo codes," *IEEE Trans. Communications*, vol. 44, no. 10, pp. 1261-1271, Oct. 1996.

[32] T. Anil-Kumar and K. D. Rao, "A new *M*–estimator base robust multiuser detection in flat-fading non-Gaussian channels," *IEEE Trans. Communications*, vol. 57, no.7, pp. 1-6, Jul. 2009.

[33] P. K. Korrai, M. N. S. Swamy, K. D. Rao, "Robust transmission of watermarked Medical image over wireless channels," *Proceedings of the IEEE GHTC,   Seattle*, *Washington*, USA, Oct. 2012.

[34] R. C. Goonzalez " Digital image processing," *Second edition, Printice Hall, Upper Saddle River, New Jersy*, USA, 2010.

101

[35] A. Paulraj, R. Nabar, D. Gore, "Introduction to space-time wireless communications," *Cambridge University Press, Cambridge*, UK, 2003.

[36] D. Gesbert, M. Shafi, D. S. Shiu, P. J. Smith, A. Naguib, From theory to practice: "an overview of MIMO space-time coded wireless systems", *IEEE Journal. Selected areas in Communications*. vol. 21, no. 3, pp. 281–302, Apr. 2003.

[37] A. Paulraj, R. Nabar, D. Gore, H. Bölcskei, "An overview of MIMO communications–a key to gigabit wireless," *Proceedings of the IEEE*, vol. 92, no. 2, pp. 198–218, Feb. 2004.

[38] IEEE Standard for Local and Metropolitan Area Networks, "Part 16: AirInterface for fixed broadband wireless access systems," IEEE Std 802. 16, Sep. 2004.

[39] IEEE Candidate Standard 802.11n: "Wireless LAN medium access control (MAC) and physical layer (PHY) Specifications," Jul. 2004.

[40] P. K. Korrai, M. N. S. Swamy, K. D. Rao, "Performance analysis of a MIMO scheme for watermarked Medical images transmission over Rayleigh fading channels," *Proceedings of the IEEE EMBS conference, Langkawi,* Malaysia, Dec. 2012.

[41] B. A. Bjerke and J. G. Proakis, "Multiple-antenna diversity techniquesfor transmission over fading channels," *Proceedings of the IEEE WCNC*, *New Orleans*, *Louisiana,* USA, pp. 1038–1042, Sep. 1999.

[42] P. W. Wolniansky, C. J. Foschini, G. D. Golden, and R. A. Valenzuela,"V-BLAST: An architecture for realizing very high data rates over the rich-scattering wireless channel," *IEEE URSI Int. Symp. Signals, Systems, and Electronics*, *Piscataway, New Jersy,*USA, pp. 295–300, Sep. 1998.

[43] G. D. Golden, C. J. Foschini, R. A. Valenzuela, and P. W. Wolniansky,"Detection algorithm and initial laboratory results using V-BLAST space-time communication architecture," *Electronics. Lett.*, vol. 35, no. 1, pp. 14–16, Jan. 1999.

[44] R. V. Nee, A. V. Zelst, and G. Awater, "Maximum likelihooddecoding in a space division multiplexing system," *Proceedings of the IEEE VTC*, *Tokyo,* Japan, May 2000.

[45] A. Burg, "VLSI Circuits for MIMO Communication Systems", *Ph.d thesis, Swiss federal institute of technology, Zurich,* Sep. 2006.

[46] K. lee, Y. Kim and J. Kang, "A novel orthogonal space-time-frequency block code for OFDM systems," *IEEE Communications. Lett.,* vol. 13, pp. 652-654, Sep. 2009.

[47] T. Chang, W. Ma and C. Chi " Maximum–likelihood detection of orthogonal space-time block coded OFDM in unknown block fading channels," *IEEE Trans. Signal Process*, vol. 56, pp. 1637-1649, Apr. 2008.

[48] S. Li, D. Huang, K. Letaief and Z. Zhou, "Pre-DFT processing for MIMO-OFDM systems with space-time-frequency coding," *IEEE Trans. Wireless communications*, vol. 6, pp. 4176-4182, Nov. 2007.

[49] H. Blocskei, M. Borgmann and A. Paulraj " Impact of the propagation environment on the performance of space-frequency coded MIMO-OFDM," *IEEE Journal. Selected areas in Communications* , vol. 21, pp. 427-439, Apr. 2003.

[50] G. J. Foschini, "Layered space-time architecture for wireless communication in a fading environment when using multiple antennas," *Bell Laboratories Technical Journal,* Vol. 1, No. 2, pp. 41-59, Mar. 1996.

[51] G. J. Foschnini and M. J. Gans, "On the limits of wireless communications in a fading environment when using Multiple Antennas," *Wireless Personal Communications,* vol. 6, no.3, pp.311-335, Aug. 1998.

[52] E. Telatar, "Capacity of multi-antenna Gaussian channels," *European Trans. Telecommunications,* vol. 6, no. 3, pp. 311-335, Dec. 1999.

[53] T. Nanji, "Reduction of implementation complexity in MIMO-OFDM decoding for V-BLAST architecture," *M. S. thesis, ECE, University of Waterloo, Waterloo*, *ON,* Canada, Aug. 2010.

[54] S. Wei, D. L. Goeckel, and M. C. Valenti, "Asynchronous cooperative diversity," *IEEE Trans. Wireless Communications*, vol. 5, pp. 1547-1557, Jun. 2006.

[55] X. Li, "Space-time coded multi-transmission among distributed transmitters without perfect synchronization", *IEEE Signal Processing. Lett.*, vol. 11, no. 12, pp. 948-951, Dec. 2004.

[56] Y. Li and X. G. Xia, "Full diversity distributed space-time codes for asynchronous cooperative communications," *IEEE International Symposium on Information Theory (ISIT), Adelaide,* Australia, pp. 911-915, Sep. 2005.

[57] Y. Shang and X. G. Xia, "Shift-full-rank matrices and applications in space-time trellis codes for relay networks with asynchronous cooperative diversity," *IEEE Trans. Information Theory*, vol. 52, pp. 3153-3167, Jul. 2006.

[58] Y. Mei, Y. Hua, A. Swami, and B Daneshrad, "Combating synchronization errors in cooperative relays," *Proceedings of the IEEE ICASSP 2005*, vol. 3, pp. 369-372, Mar. 2005.

[59] X. Li, F. Ng, and T. Han, "Carrier frequency offset mitigation in asynchronous cooperative OFDM transmissions", *IEEE Trans. Signal Processing*, vol. 56, pp. 675-685, Feb. 2008.

[60] Y. Li, W. Zhang, and X. G. Xia, "Distributive high-rate full-diversity space- frequency codes for asynchronous cooperative communications," *Proceedings of IEEE ISIT 2006, Seattle, Washington,* USA, Jul. 2006.

[61] Z. Li and X. G. Xia, "A simple Alamouti space-time transmission scheme for asynchronous cooperative systems," *IEEE Signal Processing. Lett.*, vol. 14, pp.804 - 807, Nov. 2007.

[62] Z. Li and X. G. Xia, "An Alamouti coded OFDM transmission for cooperative systems robust to both timing errors and frequency offsets", *IEEE Trans. Wireless Communications,* vol 7, pp. 1839 - 1844, May 2008.

[63] G. S. Rajan and B. S. Rajan, "OFDM based distributed space-time coding for asynchronous relay networks", *Proceedings of the IEEE ICC 2008*, *Beijing,* China, pp. 1118 - 1122, May 2008.

[64] M. Fozunbal, S. W. McLaughlin, and R. W. Schafer, "On space-time-frequency Coding over MIMO-OFDM systems", *IEEE Trans. Wireless Communications*, vol. 4, pp. 320–31, Jan. 2005.

[65] W. Su, Z. Safar, and K. J. R. Liu, "Towards maximum achievable diversity in space, time, and frequency: Performance analysis and code design," *IEEE Trans. Wireless Communications*, vol. 4, pp. 1847–57, Jul. 2005.

[66] L. Shao, S. Sandhu, S. Roy and M. Ho, "High rate space-frequency block codes for next Generation 802.11 WLANs," *Proceedings of the IEEE International conference on communications*, vol. 5, pp. 2995 – 2999, Jun. 2004.